Evaluation of the Stratospheric and Tropospheric Bromine Burden over Fairbanks, Alaska Based on Column Retrievals of Bromine Monoxide

Pamela A. Wales[1,2,3], Ross J. Salawitch [1,4,5], Elena Spinei Lind[6], George H. Mount[7], Timothy P. Canty[4], Kelly Chance[8], Sungyeon Choi[9,10], Deanna Donohoue[11], Thomas P. Kurosu[12], William R. Simpson[13], and Raid M. Suleiman[8]

[1]Department of Chemistry and Biochemistry, University of Maryland, College Park, Maryland, USA.

[2]Now at: Global Modeling and Assimilation Office, NASA Goddard Space Flight Center, Greenbelt, Maryland, USA.

[3]Now at: Universities Space Research Association, Columbia, Maryland, USA.

[4]Department of Atmospheric and Oceanic Science, University of Maryland, College Park, Maryland, USA.

[5]Earth System Science Interdisciplinary Center, University of Maryland, College Park, Maryland, USA.

[6]Department of Electrical and Computer Engineering, Virginia Polytechnic Institute and State University, Blacksburg, Virginia, USA.

[7]Laboratory for Atmospheric Research, Department of Civil and Environmental Engineering, Washington State University, Pullman, Washington, USA.

[8]Harvard-Smithsonian Center for Astrophysics, Cambridge, MA, USA.

[9]Atmospheric Chemistry and Dynamics Laboratory, NASA Goddard Space Flight Center, Greenbelt, Maryland, USA.

[10]Science Systems and Applications, Inc., Lanham, Maryland, USA.

[11]Department of Chemistry, Lawrence University, Appleton, Wisconsin, USA.

[12]NASA Jet Propulsion Laboratory and California Institute of Technology, Pasadena, CA, USA.

[13]Geophysical Institute and Department of Chemistry and Biochemistry, University of Alaska Fairbanks, Fairbanks, Alaska, USA.

Corresponding author: Pamela Wales (pamela.a.wales@nasa.gov)

Key Points:

- Retrievals of column BrO suggest upper limits for stratospheric injection of bromine from very short-lived species are 4 to 8 ppt
- Satellite retrievals are consistent with injection of 5 ppt if tropospheric BrO is 1.5×10^{13} cm^{-2} over Fairbanks, Alaska in spring 2011
- Ground-based vertical column BrO is 20% lower than satellite data and suggests tropospheric BrO is less than 1×10^{13} cm^{-2} over Fairbanks

Abstract

In spring 2011, columns of bromine monoxide (BrO) were retrieved over Fairbanks, Alaska using a ground-based multifunction differential optical absorption spectroscopy (MFDOAS) instrument. MFDOAS vertical column BrO is consistently lower than retrievals from the satellite-based Ozone Monitoring Instrument (OMI), with a relative bias of 20 ± 14%. Numerous tropical-based studies suggest that 5 ± 2 ppt of bromine from very short-lived substances (VSLS) reaches the stratosphere. We evaluate upper limits on the contribution of VSLS to stratospheric bromine by treating the column retrievals of BrO as purely stratospheric and modeling the ratio of BrO to total inorganic bromine. The OMI and MFDOAS retrievals respectively present 8 and 5 ppt upper limits on the stratospheric injection of VSLS, and kinetic uncertainties in the daytime partitioning of bromine species decrease both values by ~1.7 ppt. The OMI-based estimate is in agreement with the 5 ppt tropical-based value for stratospheric injection of VSLS if the tropospheric column of BrO is 1.5×10^{13} molecules cm^{-2} over Fairbanks, which is within the range of uncertainty of a second ground-based instrument that monitored tropospheric BrO during the campaign. Because our ground-based instruments detected no BrO near the surface, this value for tropospheric BrO would originate from higher altitudes in the troposphere and is in agreement with previous retrievals of background tropospheric BrO. Our calculations of tropospheric BrO over Fairbanks are most sensitive to uncertainties in the stratospheric loading of VSLS, followed by the difference between the OMI and MFDOAS retrievals of BrO.

1. Introduction

The role of bromine chemistry in stratospheric ozone depletion has been well established (McElroy et al., 1986; Salawitch et al., 2005; Sinnhuber & Meul, 2015; Wofsy et al., 1975). In the troposphere, inorganic bromine compounds (Br_y = BrO, Br, $BrONO_2$, HOBr, Br_2, HBr, BrCl, and $BrNO_2$) couple with chlorine and iodine catalytic cycles to alter the tropospheric oxidative capacity (Saiz-Lopez & von Glasow, 2012; Simpson et al., 2015). Furthermore, tropospheric bromine has been associated with the near-complete removal of surface ozone in the polar spring, referred to as ozone depletion events (Barrie et al., 1988). The sources and distribution of Br_y in the troposphere are an area of active research. Bromine monoxide (BrO) is the most frequently observed Br_y compound, and satellite measurements of BrO are a valuable resource for monitoring global bromine due to the extensive spatial and temporal coverage of the data (e.g., Choi et al., 2018; Schmidt et al., 2016; Wagner et al., 2001).

Tropospheric columns of BrO can be determined from satellite vertical column retrievals through a residual technique (Choi et al., 2012; Theys et al., 2011; Wagner & Platt, 1998).

Residual tropospheric BrO is calculated by removing a modeled, stratospheric column from the retrieved, total vertical column density of (BrO^{VCD}). Thus, an accurate understanding of stratospheric BrO is first required to calculate tropospheric BrO from satellite measurements. Simulations of stratospheric BrO are dependent on the partitioning of stratospheric Br_y into BrO (i.e., the BrO/Br_y ratio) as well as the amount of Br_y in the stratosphere (Salawitch et al., 2010; Sioris et al., 2006; Theys et al., 2009). In this study, we quantify upper limits for the stratospheric loading of Br_y using satellite and ground-based measurements of BrO^{VCD} collected over Fairbanks, Alaska in spring 2011. Additionally, we evaluate the sensitivity of satellite-based estimates of BrO in the troposphere to uncertainties in measurements of BrO^{VCD}, the stratospheric loading of Br_y, and the kinetics regulating the BrO/Br_y ratio.

Long-lived compounds (halons and CH_3Br) as well as naturally produced very short-lived substances (VSLS) deliver bromine to the stratosphere (Ko et al., 2003; Wales et al., 2018). The amount of stratospheric Br_y supplied by VSLS (Br_y^{VSLS}) is the largest source of uncertainty to the stratospheric loading of Br_y. Brominated VSLS are organic compounds ($CHBr_3$, CH_2Br_2, CH_2BrCl, $CHBr_2Cl$, and $CHBrCl_2$) that are primarily emitted by marine biological activity and have tropospheric lifetimes less than 6 months (Ko et al., 2003). Due to their short lifetimes, brominated VSLS partially decompose in the troposphere, forming inorganic product gases that are readily available to participate in ozone depletion upon entering the stratosphere. Furthermore, because heterogeneous reactions on aerosol surfaces increase the efficiency of bromine-mediated ozone loss, the impacts on stratospheric ozone of major volcanic eruptions and geoengineering via stratospheric injection of aerosols are both sensitive to Br_y^{VSLS} (Klobas et al., 2017; Salawitch et al., 2005; Tilmes et al., 2012).

Both VSLS and their inorganic product gases enter the stratosphere primarily through the tropical tropopause layer **(Aschmann et al., 2009; Chen et al., 2016; Koenig et al., 2017)**. Based on measurements of BrO and numerous observations of VSLS in the tropical tropopause layer, VSLS are expected to contribute 5 ± 2 ppt of bromine to the stratospheric (e.g., Dorf et al., 2008; Engel et al., 2018; Wales et al., 2018). Currently, VSLS supply about 25% of the bromine in the stratosphere, and their relative contribution to stratospheric bromine will increase as mixing ratios of regulated anthropogenic source gases decline (Engel et al., 2018).

Past studies have attempted to determine Br_y^{VSLS} as well as the total loading of stratospheric Br_y based on measurements of BrO in stratospherically aged air. These studies made use of either ground-based (e.g., Schofield, 2004; Theys et al., 2007), balloon-borne (e.g., Dorf et al., 2008; Stachnik et al., 2013), or satellite instruments (e.g., Kovalenko et al., 2007; Millán et al., 2012; Parrella et al., 2013; Salawitch et al., 2010; Sinnhuber et al., 2005; Sioris et al., 2006) to measure stratospheric BrO. The stratospheric loading of Br_y was determined by modeling the BrO/Br_y ratio. These older studies had produced a wide range of estimates for Br_y^{VSLS} (3 to 9 ppt). The mean value of these estimates is 6 ppt (Table 1-14 in Montzka et al., 2011), slightly higher than the 5 ppt expected from measurements of VSLS in the tropics (Dorf et al., 2008; Engel et al., 2018; Wales et al., 2018). However, estimates of Br_y^{VSLS} from stratospheric measurements of BrO are sensitive to the modeled kinetics that govern the BrO/Br_y ratio as well as instrumental uncertainties in the measurements of BrO (e.g., McLinden et al., 2010; Parrella et al., 2013; Salawitch et al., 2010; Sioris et al., 2006).

The stratospheric BrO/Br_y ratio is largely governed by mixing ratios of NO_2 as well as the rates of formation and photolysis of $BrONO_2$ (Sioris et al., 2006; Theys et al., 2009). In the lower stratosphere, the majority of daytime Br_y cycles between $BrONO_2$ and BrO via the formation of $BrONO_2$ through a three-body reaction, dependent on the density of air (M):

$$BrO + NO_2 + M \rightarrow BrONO_2 + M \tag{1}$$

as well as the photolysis of $BrONO_2$:

$$\begin{aligned} BrONO_2 + h\nu &\rightarrow BrO + NO_2 \\ &\rightarrow Br + NO_3 \\ &\rightarrow BrO + NO + O(^3P) \end{aligned} \tag{2}$$

All production pathways of reaction (2) rapidly feed into the reactive bromine (Br + BrO) cycle.

Kreycy et al. (2013) suggested modifications to the photolysis frequency of $BrONO_2$ (J_2) relative to the rate constant of $BrONO_2$ formation (k_1). In their study, twilight observations of O_3, NO_2, and BrO were collected in the lower stratosphere using a balloon-borne differential optical absorption spectroscopy (DOAS) instrument. These measurements focused on the lower stratosphere where the BrO/Br_y ratio is most sensitive to reactions (1) and (2). The observed BrO formed more quickly in the morning and decreased more slowly in the evening than predicted by model simulations. Consequently, Kreycy et al. (2013) proposed that the 2011 NASA Jet Propulsion Laboratory (JPL 2011) kinetic values (Sander et al., 2011) underestimate the ratio of J_2/k_1 at 220 ± 5 K by 70%. The proposed modification to the kinetics that govern formation and loss of $BrONO_2$ is well within the uncertainties of laboratory measurements but was not supported by twilight measurements of $BrONO_2$ over midlatitudes (Wetzel et al., 2017). If implemented in the stratosphere, these kinetic adjustments to reactions (1) and (2) would increase the daytime BrO/Br_y ratio and decrease the amount of Br_y^{VSLS} needed to explain stratospheric measurements of BrO.

In this study, we reconcile estimates of Br_y^{VSLS} based on measurements of BrO collected in stratospherically aged air with tropical tropopause-based estimates by systematically considering uncertainties unique to the stratospheric approach. We use a stratospheric box model, described in Section 2.3, to systematically test the sensitivity of estimates of Br_y^{VSLS} to kinetic uncertainties in reactions (1) and (2). In Section 3.1, we present retrievals of BrO^{VCD} collected over Fairbanks, Alaska by the Ozone Monitoring Instrument (OMI) onboard the NASA Aura satellite (Veefkind et al., 2006) by and a ground-based multifunction DOAS (MFDOAS) instrument during March and April 2011. In Section 3.2, we describe ground-based multi-axis DOAS (MAX-DOAS) observations that monitored tropospheric BrO over Fairbanks during the campaign.

The OMI and MFDOAS retrievals of BrO^{VCD} do not provide information concerning the vertical distribution of BrO over Fairbanks. Additionally, because the tropospheric signal of BrO detected by the MAX-DOAS instrument originates from altitudes above the location of the instrument, the MAX-DOAS technique is not able to accurately quantify the profile and mixing ratio of tropospheric BrO during the campaign (e.g., Frieß et al., 2011). Consequently, in Section 3.3, we first treat the OMI and MFDOAS retrievals of BrO^{VCD} as purely stratospheric to constrain the upper limits of Br_y^{VSLS}. In Section 3.4, we consider the role of free tropospheric BrO in deriving estimates of Br_y^{VSLS} from retrievals of BrO^{VCD} and demonstrate the sensitivity of tropospheric residual BrO calculations to stratospheric uncertainties.

2. Instrument and Model Description

2.1. Fairbanks 2011 Campaign

The 2011 Fairbanks BrO campaign was located at the University of Alaska, Fairbanks (64.86°N, 212.15°E). Three different DOAS instruments were deployed during the campaign: the Washington State University MFDOAS instrument (Herman et al., 2009; Spinei et al., 2010), two NASA Pandora instruments (Tzortziou et al., 2012), and the University of Alaska, Fairbanks MAX-DOAS instrument (Peterson et al., 2015; Simpson et al., 2017). The MFDOAS instrument measured UV and visible spectra from the direct sun and multi-axis observation geometries from 23 March through 8 April 2011 with a U340 blocking filter that eliminated scattered light from wavelengths greater than approximately 350 nm. Direct sun measurements provide values of BrO^{VCD} derived from spectral analysis and a simple geometric determination of the air mass factor, while the multi-axis data are mainly sensitive to BrO present in the lower troposphere and involves a more complicated determination of the air mass factor. The Pandora instruments measured only in the direct sun mode, but due to spectral interference from the front window on the Pandora instrument, BrO absorption levels were often below the Pandora detection limit. All three instruments are capable of collecting data that are used in DOAS retrievals of BrO, NO_2, and O_3.

Our model setup utilizes measurements of O_3 and temperature acquired by balloon-borne ozonesondes during the 2011 campaign (Johnson et al., 2018). Total column measurements of O_3 were collected by a Brewer spectrometer on 24 March through 4 April (Tzortziou et al., 2012). Ozonesondes were launched daily between 25 March and 8 April around 11:00 am local solar time. On 1 April the balloon burst near 11 km, but for all other days of the campaign the balloon reached an altitude of ~30 km. Only observations collected below 20 km are used to constrain the box model and define tropopause pressure, as described in Section 2.3.

2.1.1. MFDOAS Instrumentation

MFDOAS is a research grade instrument that has been used in the validation of OMI NO_2 and SO_2 columns (Herman et al., 2009; Spinei et al., 2010). The MFDOAS instrument version utilized in 2011 had two separate telescopes to perform measurements in the direct sun and the multi-axis observation geometries. The instrument observing strategy during this campaign concentrated on direct sun measurements. Table 1 lists the gas species and references to the molecular cross sections used in the MFDOAS BrO fitting.

The retrieval of BrO from both ground and satellite-based atmospheric spectra is complicated due to the relatively small atmospheric abundance of BrO and the near UV spectral cross correlation of BrO with abundant molecules, such as NO_2, that strongly populate the observed spectrum. Additionally, the cross sections of weak potential atmospheric absorbers, formaldehyde (CH_2O) and chlorine dioxide (OClO), are highly correlated with the BrO spectral absorption cross sections. The DOAS fitting of atmospheric spectra to the molecular cross section spectra is performed using a third-order polynomial as well as a zero and first-order non-linear offset to correct for stray light interferences. No Ring spectra were used in the fitting since the observations were of the direct sun. The focal plane pixel sampling of the full width at half maximum of the instrument profile was well defined at 7.5 detector pixels, the reduction spectral residual root mean squared was typically a few hundredths of a percent, and the wavelength calibration was performed using atomic emission and solar Fraunhofer lines with an accuracy < 0.01 nm.

Table 1. Molecular absorption cross sections used in the MFDOAS BrO sensitivity study.

Species	Temperature (K)	Source
O_3	218 and 243	(Brion et al., 1993; Malicet et al., 1995)
NO_2	220	(Vandaele et al., 1998)
O_2-O_2	296	(Hermans et al., 1999)
OClO	204	(Wahner et al., 1987)
BrO	228	(Wilmouth et al., 1999)
CH_2O	298	(Meller & Moortgat, 2000)

The value of BrO^{VCD} is determined from direct sun measurements by first estimating the amount of BrO in the reference spectrum and then dividing the slant column density (SCD) by a simple direct sun geometrical air mass factor (AMF) that does not require radiative transfer calculations. The SCD in the reference spectrum was determined using a minimum extrapolation Langley method. To evaluate the error of BrO^{VCD} to the amount in the reference spectrum, different SCD data percentiles were utilized for the Langley fit. This is the second largest source of error in the MFDOAS BrO^{VCD} calculation, after the spectral fitting scenario. The AMF error is less than 1% for the direct sun observations at solar zenith angles (SZA) smaller than 80°.

Multiple DOAS reduction scenarios were used to evaluate BrO SCD errors to determine the optimal fitting scenario for the MFDOAS direct sun retrieval of BrO in Fairbanks. The parameters varied in these reduction scenarios include: the spectral fitting window, polynomial order, the ozone cross section temperatures, the offset correction for stray light (small due to inclusion of a U340 cutoff filter), as well as the inclusion of CH_2O and OClO absorption cross sections. The sensitivity of the MFDOAS retrieval of BrO to the DOAS fitting parameters is summarized in Table S1.

Overall, the DOAS wavelength fitting window is the largest source of uncertainty in the MFDOAS retrieval of BrO^{VCD} during the campaign (Table S1). To demonstrate the sensitivity of BrO^{VCD} to the spectral fitting window, Figure 1 shows BrO^{VCD} collected on 3 April for five wavelength windows reduced using the same raw data. The error bars associated with the MFDOAS measurements in Figure 1 are the uncertainties in BrO^{VCD} from the Langley fit. MFDOAS retrievals for the whole campaign are shown in supporting information Figure S1. For the results presented in Section 3, the reported MFDOAS values of BrO^{VCD} are determined from direct sun observations using the 336 – 359 nm fitting window, shown in red in Figure 1. This spectral fitting window is sensitive to the inclusion of the CH_2O cross section. To reduce errors in the retrieval due to correlations between these cross sections, the cross sections of CH_2O and OClO are orthogonalized relative to the BrO cross section using the method described in Spinei et al. (2014). The 336 – 359 nm wavelength range was chosen as the optimal fitting window for the MFDOAS instrument because this window minimizes the correlation of the BrO spectra with other absorbing species, reduces the sensitivity of the retrieval to the DOAS fitting parameters listed in Table S1, and produces a physically realistic diurnal variation of BrO^{VCD}.

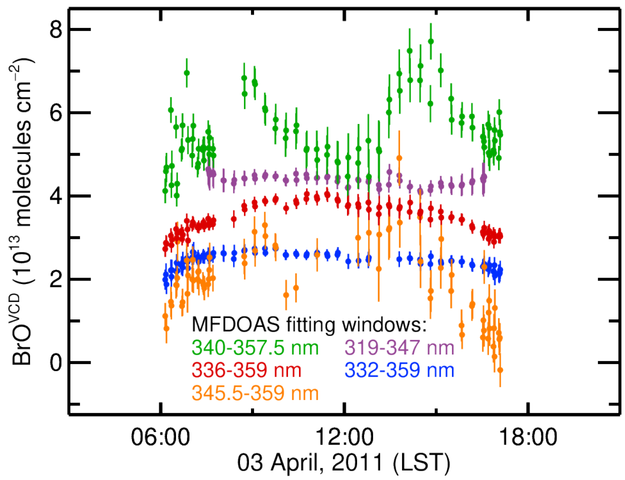

Figure 1. Values of BrO^{VCD} over Fairbanks, Alaska on 3 April 2011 from OMI and from five different retrievals using the same MFDOAS direct sun data. The error bars represent the 1σ uncertainty due to the Langley fit.

Under stable atmospheric conditions, daytime BrO^{VCD} is expected to change gradually with time (see Section 3.3 for further details). Values of BrO^{VCD} retrieved by the 340 – 357.5 nm (green in Figure 1) and 345.5 – 359 nm (orange) windows are rejected from our analysis, because for most days during the campaign retrievals from these spectral windows produce large, unrealistic diurnal variations indicating the influence of absorbances from strongly absorbing interfering species, such as NO_2. The diurnal variation in BrO^{VCD} collected by the other three fitting windows are relatively stable. Therefore, we define the uncertainty in MFDOAS BrO^{VCD} due to the selection of the spectral fitting window using the range of BrO^{VCD} retrieved from the 332 – 359 nm (blue) and 319 – 347 nm (purple) spectral fitting windows. This results in a 1σ uncertainty of 0.4 × 10^{13} molecules cm^{-2} centered on the 336 – 359 nm wavelength fitting window. For the results presented in Section 3.1, we apply a five-minute average to the MFDOAS retrievals of BrO^{VCD}, and the reported uncertainty in the MFDOAS observations is the combination in quadrature of the standard deviation about the 5 min mean, the 1σ fitting uncertainty due to the Langley fit (shown in Figures 1 and S1), and the 1σ fitting uncertainty due to the DOAS spectral fitting window.

2.1.2. MAX-DOAS Instrumentation

The University of Alaska, Fairbanks MAX-DOAS instrument monitored tropospheric BrO during the spring 2011 campaign. This instrument is described by Peterson et al. (2015) and Simpson et al. (2017). The MAX-DOAS spectral fitting technique calculates the differential SCD (dSCD) of absorbing gases along lower elevation views relative to a zenith reference spectrum collected within the same elevation scan. Because most light scattering occurs below the stratosphere, both the low elevation and zenith spectra share similar stratospheric paths. Consequently, the retrieved dSCD has low sensitivity to BrO in the stratosphere and the upper troposphere (Honninger & Platt, 2002).

During the 2011 campaign, the MAX-DOAS instrument scans at elevation angles of 2, 5, 10, 20, and 90° above the horizon every ~30 min. Values for dSCDs of BrO are retrieved from the MAX-DOAS spectra using a 337 – 364 nm wavelength fitting window. This wavelength range is similar to the MFDOAS 336 – 359 nm optimal fitting window but includes a large peak of the O_2-O_2 collision complex (O_4) at 361 nm. Including this O_4 peak improves the quantification of the effective pathlength from the MAX-DOAS observations. The spectra are fitted with a third order polynomial using absorption cross sections listed in Simpson et al. (2017). The same trace gases as the MFDOAS instrument are considered in the MAX-DOAS fitting (Table 1), with the exception of OClO. The OClO absorption cross section is not included in the MAX-DOAS retrieval, because OClO is a mostly stratospheric absorber. Consequently, since the reference spectra are collected by the zenith viewing geometry, OClO absorption does not impact dSCD retrievals. Because all retrievals of BrO from the MAX-DOAS instrument are reported relative to the zenith spectra, the resulting dSCD of BrO is less sensitive to the DOAS fitting parameters than the direct sun data collected by the MFDOAS instrument. The zenith reference removes the influence of stratospheric absorbers by an order of magnitude at twilight and significantly reduces the dependence on the DOAS fitting window.

The analysis presented in Section 3 is restricted to MAX-DOAS spectra collected at SZAs less than 75° during clear-sky conditions. Because the presence of clouds reduces the dSCD of O_4 relative to clear-sky retrievals, only MAX-DOAS data collected when dSCD of O_4 at the 20° elevation angle is greater than 1.5×10^{43} molecules^2 cm^{-5} is included in Section 3.

2.2. The Ozone Monitoring Instrument (OMI)

OMI is an ultraviolet-visible, nadir viewing instrument onboard the NASA Earth Orbiting System-Aura satellite. The Aura satellite is in a sun-synchronous, polar orbit with an equatorial crossing time of 13:45 in the ascending node. The OMI swath width is 2600 km with a 13×24 km^2 spatial resolution at the center of the swath (Levelt et al., 2006). Due to the high latitude location of Fairbanks, multiple OMI overpasses at varying time of day are available for most days during the campaign.

Retrievals of BrO^{VCD} from OMI are calculated from the slant column measurements using direct fitting of the radiances. The current OMI BrO retrieval (version 3.0.5) uses a wavelength fitting window of 319 – 347.5 nm and BrO cross sections at 228 K from Wilmouth et al. (1999). Slant and vertical column densities of BrO are calculated following spectral fitting of BrO, Ring scattering, O_3, NO_2, CH_2O, OClO, and SO_2. The OMI retrieval determines BrO^{VCD} using a wavelength and albedo dependent AMF that is calculated prior to spectral fitting (Suleiman et al., 2019). This AMF depends on a number of factors including the assumed profile of BrO, surface albedo, and the modeled wavelength dependence, as discussed in Suleiman et al. (2019). For each orbit, we average level 2 data within a 200 km radius of Fairbanks, weighted by the inverse of the distance to Fairbanks. The reported error in BrO^{VCD} is the combination of 1σ uncertainties in the random spectral fitting uncertainty (Suleiman et al., 2019) and the standard deviation about the 200 km radius mean.

The box model described in Section 2.3 is constrained to OMI measurements of column O_3 and NO_2. Observations of total column O_3 and reflectivity from OMI are taken from the level 3 DOAS product (Veefkind et al., 2006). We use the NASA OMI level 2 stratospheric column NO_2 (Bucsela et al., 2013; Krotkov et al., 2017) to constrain modeled nitrogen oxides. OMI stratospheric columns NO_2 are estimated over unpolluted regions using a tropospheric climatology (Bucsela et al., 2013). The uncertainty in OMI stratospheric column NO_2 is a minor contribution to uncertainties in our results (Section 3.2.1).

2.3. Stratospheric Box Model

In this section, we describe the stratospheric box model that is used in Section 3.3 to investigate the impact of kinetic uncertainties in reactions (1) and (2) and constrain the upper limits of Br_y^{VSLS} over Fairbanks. The box model includes 187 reactions and 37 chemical compounds. Rate constants and absorption cross sections are defined according to the JPL kinetic evaluation (Burkholder et al., 2015). The mechanism within the box model has been extensively tested and compared with global model simulations and observations (SPARC, 2010). Profiles of photolysis frequencies and rate constants are calculated over Fairbanks, Alaska (64.86°N, 212.15°E) in 15 min intervals for a full diel cycle. The partitioning of Br_y compounds are calculated assuming photochemical steady state over the diel cycle. Long-lived chemical and physical tracers are constrained in model as described in Section 2.3.1. We consider seven scenarios for the stratospheric loading of Br_y^{VSLS} and five kinetic scenarios as described in Section 2.3.2 and Section 2.3.3, respectively.

This model calculates stratospheric columns of BrO over Fairbanks for 25 March through 8 April 2011 (Salawitch et al., 2010; Wales et al., 2018) for the period of ground-based retrievals of column BrO. Profiles of BrO are modeled for each value of Br_y^{VSLS} and kinetic scenario. Stratospheric BrO^{VCD} is calculated by integrating the modeled profiles of BrO from the tropopause pressure to 0.01 hPa. For each day, the tropopause pressure is calculated using the measured ozonesonde temperature profiles according to the thermal lapse rate definition for tropopause pressure given by the World Meteorological Organization (1957). During the campaign, the ozonesonde-based tropopause is in close agreement with the tropopause pressure reported by GMI for all days where daytime MFDOAS measurements are collected (Figure S2).

2.3.1. Model Constraints

The box model is constrained to profiles of long-lived chemical and physical tracers from the NASA Global Modeling Initiative (GMI) chemical transport model (Strahan et al., 2007). The GMI model was constrained to reanalysis meteorological fields from Modern-Era Retrospective Analysis for Research and Application (MERRA; Rienecker et al., 2011). Daily GMI profiles of temperature, O_3, total reactive nitrogen (NO_y), CH_4, CO, H_2O, inorganic chlorine (Cl_y), N_2O, and CFC-11 are used to constrain long-lived tracers in the box model. The GMI variables are provided on a 2° latitude and 2.5° longitude grid with 72 vertical levels and are interpolated to the latitude and longitude of the location of the University of Alaska, Fairbanks (64.86°N, 212.15°E).

Stratospheric aerosol surface area density in the box model is constrained to monthly, zonal mean profiles prepared for the Chemistry-Climate Model Initiative (CCMI). The CCMI aerosol dataset is based on 532 nm backscatter measurements from Cloud-Aerosol Lidar and Infrared Pathfinder Satellite Observations (CALIPSO) and is available on 1° latitude bins with

72 vertical levels (Eyring et al., 2013). Profiles of aerosol surface area density are interpolated to the latitude of Fairbanks and the pressure levels of the GMI output.

Model constraints are further refined using OMI data and ozonesonde observations collected during the ground campaign. Photolysis frequencies are calculated using OMI total column O_3 and reflectivity. Below 20 km, the box model is constrained to the observed ozonesonde profiles of temperature and ozone measured during the Fairbanks campaign. Box model profiles of O_3 above 20 km, initially constrained to GMI output, are linearly scaled so that modeled total column O_3 matches OMI observations. Additionally, profiles of NO_y in the box model, initially constrained to GMI output, are scaled linearly so that box modeled stratospheric columns of NO_2 are within 1% of OMI observations of column NO_2.

Finally, profiles of Br_y are calculated using GMI CFC-11 and N_2O following the method described in Wales et al. (2018). In the stratosphere, VSLS and long-lived, organic bromine compounds (CH_3Br and halons) decompose forming Br_y. CFC-11 and N_2O are species with long photochemical lifetimes that slowly decay in the stratosphere and can be used as tracers for the mean age of air (e.g., Engel et al., 2002; Wamsley et al., 1998). We use values of CFC-11 from GMI as a stratospheric tracer to calculate the formation of Br_y due to the decomposition of organic source species as air ages in the stratosphere. Due to regulations under the Montreal Protocol, mixing ratios of CH_3Br and halons have decayed by ~10 % (i.e., 1.7 ppt) between 2011 and the peak halogen loading in 1999. We account for the slightly higher bromine content in older stratospheric air using GMI values of N_2O and the mean age of air parameterization as a function of N_2O developed in Engel et al. (2002). We do not expect uncertainties in this parameterization or GMI N_2O to have a strong effect on our calculations of Br_y.

The majority of inorganic bromine forms below 20 km. To represent the effect of dynamics in the lower stratosphere over Fairbanks during spring 2011, we adjust GMI profiles of CFC-11 and NO_y using the observed ozonesonde measurements of O_3. Mixing ratios of CFC-11 and O_3, simulated over Fairbanks for March and April 2011, are negatively correlated in GMI, while mixing ratios of NO_y and O_3 are positively correlated in GMI. Both correlations are well represented using quadratic fits (Figure S3). Using the quadratic fit, shown in Figure S3a, we calculate CFC-11 using ozone mixing ratios from the ozonesondes. This process is also used for profiles of NO_y, prior to the scaling NO_y to match OMI stratospheric columns of NO_2. These ozonesonde-based adjustments to the profiles of CFC-11 and NO_y have only a minor impact on the scientific results of our study.

2.1.2. Br_y^{VSLS} Scenarios

The model is constrained to profiles of Br_y for seven possible contributions of VSLS. For one scenario, we neglect the stratospheric contribution of VSLS and calculate Br_y using only long-lived source gases (Br_y^{VSLS} = 0 ppt). A second scenario assumes only a stratospheric supply of Br_y from source gas injection (SGI) of long-lived bromocarbons and VSLS. Based on the aircraft observations described by Wales et al. (2018), the contribution of VSLS to stratospheric bromine via SGI is expected to be 2.9 ppt (which we term Br_y^{VSLS} = 3 ppt for simplicity). The remaining five scenarios consider contributions of direct injection of Br_y (i.e., product gas injection, PGI) in 2 ppt increments (Br_y^{VSLS} = 5 to 13 ppt). To represent PGI, we add constant amounts of Br_y (2 to 10 ppt) to the profiles calculated from the stratospheric CFC-11 tracer relation. The range of Br_y^{VSLS} extends to 13 ppt only to simulate BrO^{VCD} above the upper limits of OMI BrO^{VCD}, and box model results for Br_y^{VSLS} = 11 and 13 ppt are not shown in Section 3.

2.1.2. Kinetic Scenarios

For our base kinetic scenario, profiles of BrO are modeled for each value of Br_y^{VSLS} using the kinetic recommendations given by JPL (Burkholder et al., 2015). We conduct four additional kinetic scenarios to test the sensitivity of our results to the various kinetic recommendations for $BrONO_2$ formation (k_1) and photolysis (J_2). To model the kinetic recommendations given in Kreycy et al. (2013), we decrease the JPL value for k_1 by a factor of 0.75 and increase J_2 by a factor of 1.27. We refer to this kinetic scenario as Scaled (J & k). The differences between the $BrONO_2$ kinetic recommendations in JPL 2011 (Sander et al., 2011), used by Kreycy et al. (2013), and JPL 2015 (Burkholder et al., 2015), used in our study, are negligible.

We also run three simulations using $BrONO_2$ kinetics from IUPAC (Atkinson et al., 2007). With all other kinetic parameters defined by JPL, we use the IUPAC recommendation for $BrONO_2$ cross sections for one set of simulations. For a second run, the rate constants for reaction (1) are defined by IUPAC. A final run uses IUPAC kinetic parameters for both reactions (1) and (2). We refer to these three kinetic scenarios as IUPAC (J), IUPAC (k) and IUPAC (J & k), respectively.

Values of k_1 recommended by JPL, IUPAC, and three laboratory studies are shown in supporting information Figure S4. The JPL recommendation for k_1 is based on a least-squares fit to laboratory data from the Thorn et al. (1993) and Sander et al. (1981) studies. For IUPAC recommendations, the low-pressure limit for k_1 in IUPAC is based on the Thorn et al. (1993), Sander et al. (1981), and Danis et al. (1990) laboratory studies, while the high-pressure limit is temperature independent and derived from measurements at 298 K from the Thorn et al. (1993) and Sander et al. (1981) studies.

At standard temperature and pressure, the JPL and IUPAC recommendation for k_1 are in close agreement. However, the k_1 low-pressure limit calculated from the Danis et al. (1990)

study is smaller than the extrapolation of the Thorn et al. (1993) measurements. The JPL recommendation for k_1 does not incorporate values from Danis et al. (1990), and notes that the slower rate constants reported by Danis et al. (1990) could be due to heterogeneous loss of NO_2 in their reactor setup (Burkholder et al., 2015; Thorn et al., 1993). As a result, the IUPAC values for k_1, which include the Danis et al. (1990) study, are consistently smaller than JPL at stratospheric pressures. Additionally, the temperature-independent k_1 high-pressure limit used by IUPAC results in even smaller values of k_1 than JPL in the lower temperatures found in the lower stratosphere. The values for k_1 shown in Figure S4 are calculated using density of air equal to 1.6 $\times$ 10^{18} molecules cm^{-3} to demonstrate conditions around 20 km, where the Br_y partitioning is most sensitive to $BrONO_2$ kinetics. When the density of air is 1.6 $\times$ 10^{18} molecules cm^{-3}, the IUPAC recommendation for k_1 is 16% smaller than JPL at 298 K and 33% smaller at 220 K.

Values of the $BrONO_2$ cross section (σ_2), used to calculate J_2, are shown in supporting information Figure S5. For the photodissociation of $BrONO_2$, the JPL and IUPAC recommendations for σ_2 are nearly identical at room temperature. At 220 K, the IUPAC values for σ_2 are larger than the JPL recommendation at wavelengths greater than 300 nm. For this cross section, the JPL recommendation is based on the laboratory measurements by Burkholder et al. (1995), while the IUPAC recommendation averages data from the Burkholder et al. (1995) and Deters et al. (1998) studies.

2.4. Calculating Tropospheric Column BrO from OMI Observations and Modeled Stratospheric BrO

Tropospheric columns of BrO are calculated from OMI retrievals of total BrO^{VCD} using the tropospheric residual method (Choi et al., 2012; Theys et al., 2011; Wagner & Platt, 1998). As discussed in Section 2.2, the vertical column density (VCD) of OMI BrO is calculated from the SCD observations by applying a wavelength-dependent, mostly stratospheric AMF prior to spectral fitting. The OMI retrieval determines the SCD of BrO through spectral fitting without applying the wavelength-dependent AMF. An effective AMF is provided in the OMI product (AMF_{OMI}) based on the ratio between the retrieved SCD and VCD, according to equation 3 (Suleiman et al., 2019).

$$AMF = \frac{SCD}{VCD} \tag{3}$$

Since the sensitivity of the satellite instrument to the signal of BrO depends on the profile shape of the absorbing species, tropospheric AMFs (AMF_{Trop}) must be included to accurately calculate tropospheric VCD. We calculate AMF_{Trop} with scattering weight profiles prepared using the Linearized Discrete Ordinate Radiative Transfer model (LIDORT; Spurr et al., 2001) by Choi et al. (2012). As discussed in Section 3.2, tropospheric BrO was not detected near the surface over Fairbanks during the 2011 campaign. Thus, we follow the procedure described by Choi et al. (2012) to calculate AMF_{Trop} from the scattering weight profile and assuming the tropospheric profile of BrO is a constant mixing ratio between 2 km and the tropopause and is 0 ppt below 2 km. Under clear-sky conditions AMF_{Trop} is calculated as a function of SZA, the viewing zenith angle (VZA) of OMI, surface albedo reported by the OMI DOAS O_3 product, and tropopause height. Under cloudy-sky conditions AMF_{Trop} is calculated as function of SZA, VZA, cloud height, and tropopause height. Surface albedo and cloud height are from OMI measurements within 200 km of Fairbanks. Clear and cloudy-sky AMF_{Trop} calculations are averaged, weighted by the OMI cloud fraction.

For each OMI overpass, tropospheric BrO^{VCD} is calculated from OMI total column BrO and modeled stratospheric column BrO. Stratospheric BrO^{VCD} is modeled over Fairbanks with a 15 minute temporal resolution according to the methods described in Section 2.3. Modeled stratospheric BrO^{VCD} is linearly interpolated over time to the time of each OMI overpass. The resulting stratospheric BrO^{VCD} is multiplied by the stratospheric-based AMF_{OMI} to determine stratospheric SCD. The tropospheric SCD is the difference between the OMI total SCD and modeled stratospheric SCD. The resulting quantity is divided by the LIDORT-derived AMF_{Trop} to calculate tropospheric VCD:

$$VCD_{Trop} = \frac{SCD_{OMI} - VCD_{Strat} \times AMF_{OMI}}{AMF_{Trop}} \qquad (4)$$

3. Results and Discussion

3.1. MFDOAS and OMI Measurements of Vertical Column BrO

Measurements of BrO^{VCD} from OMI and MFDOAS over Fairbanks, Alaska collected during spring 2011 are shown in Figure 2. In Figure 2, MFDOAS direct sun observations are 1 hour averages, centered at the time of each daytime OMI overpass. The error bars for MFDOAS are the combination in quadrature of the DOAS 1σ fitting uncertainty, uncertainty in the spectral fitting window, and the standard deviation about the 1 hour mean, as described in Section 2.1. The OMI error bars are the 1σ fitting uncertainty, described in Section 2.2.

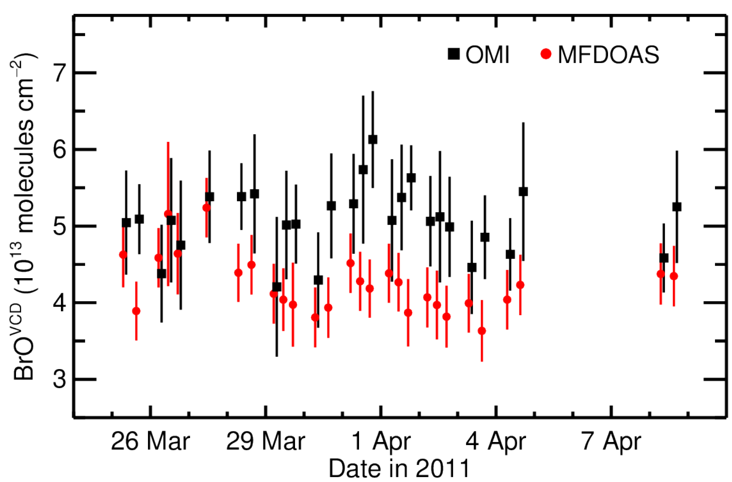

Figure 2. Simultaneous measurements of BrO^{VCD} over Fairbanks, Alaska obtained by OMI and MFDOAS. (a) Black squares are daytime OMI observations of BrO^{VCD}, and error bars are the reported 1σ total measurement uncertainty. Red points are MFDOAS direct sun observations, averaged for 1 hour around each OMI retrieval. The error bars for MFDOAS are the root sum of squares combination of the DOAS fitting uncertainty, uncertainty in the spectral fitting window, and the standard deviation of the measurements within 1 hour of each OMI observation.

Only observations collected at SZAs less than 70° and within 30 min of each other are shown in Figure 2. Daytime (SZA < 70°) MFDOAS measurements were not collected on 6 and 7 April. Since daytime determinations of OMI and MFDOAS BrO^{VCD} on 5 April were not acquired within 30 min of each other, these observations are not shown in Figure 2. However, measurements of BrO^{VCD} on 5 April are included in Sections 3.3 and 3.4. For all days except 26 March, the MFDOAS retrievals of BrO^{VCD} are lower than those reported by OMI. The average and standard deviation of the relative bias between the OMI and MFDOAS retrievals of BrO^{VCD} is 20 ± 14% during the campaign.

Retrievals of BrO^{VCD} from the MFDOAS instrument are determined using the DOAS method to separate the relatively weak signal of BrO from interfering absorbers (Stutz & Platt, 1996), while BrO^{VCD} from the OMI instrument is calculated through a direct nonlinear least squares fitting of the measured radiances. For both methods, the choice of fitting window must balance the stronger absorption and unique spectral structure of BrO with minimal interference from other atmospheric absorbers (Platt & Stutz, 2008). Datasets from various instruments may require different fitting windows for optimal retrieval due to differences in instrumental properties (e.g., spectral efficiency, spectral line shape, spectral resolution and sampling) as well as detector noise and radiative transfer processes.

Past studies have compared OMI measurements of BrO^{VCD} over Harestua, Norway (60°N, 11°E) to ground-based DOAS observations for 2005 through 2011 (Choi et al., 2018; Suleiman et al., 2019). The ground-based measurements of BrO^{VCD} at Harestua were collected using a zenith-sky DOAS instrument and a fitting window of 345 – 359 nm (Hendrick et al., 2007). Suleiman et al. (2019) analyzed daily mean observations of BrO^{VCD} for February through August for years 2005 to 2011 over Harestua and report a small, relative bias of 3 ± 16 %, much lower than the 20 ± 14 % bias we report over Fairbanks based on the MFDOAS ground-based data. Choi et al. (2018) analyzed March and April twilight observations of BrO^{VCD} from the Harestua ground-based instrument in the evening, which provides sensitivity to the tropospheric and stratospheric component of the BrO profile. After converting the ground-based measurements of BrO^{VCD} to the OMI overpass time using a photochemical box model (Hendrick et al., 2007), the relative bias of the OMI to ground-based BrO^{VCD} was found to be 13 ± 12 %. The relative bias of OMI to MFDOAS BrO^{VCD} over Fairbanks is higher than both values but within the standard deviation of the Choi et al. (2018) study.

3.2. MAX-DOAS Measurements of Tropospheric BrO

The MAX-DOAS technique is most sensitive to atmospheric layers close to the instrument's altitude. By scanning at low elevation angles above the horizon, high sensitivity to the lower troposphere is achieved because slant path lengths are long at small elevation angles (Honninger & Platt, 2002). During the Fairbanks campaign, the 2° elevation angle was clear of obstructions and provided high sensitivity to BrO within 300 m above the ground level. Scans performed with larger elevation angles sample gases at higher altitudes, but the slant path length through the troposphere becomes progressively shortened as the elevation angle increases. Previous studies indicate that the ability of MAX-DOAS methods to quantify the mixing ratio and altitude of BrO is significantly degraded above 2 km (Frieß et al., 2011; Peterson et al., 2015). As a result, the UAF MAX-DOAS data collected during the Fairbanks campaign is analyzed in two ways. First, surface mixing ratios of BrO are calculated from the 2° elevation angle scans. Second, the full elevation scan is used to qualitatively examine the vertical distribution of BrO over Fairbanks.

The surface mixing ratio of BrO is evaluated using a scaling technique (Stutz et al., 2017). The surface mixing ratio of BrO ($X_{BrO,surf}$) is quantified using the relative abundance of BrO to O_4. Because the MAX-DOAS viewing path at a 2° elevation angle only rises ~300 m before light scatters, the amount of O_4 within this path is equal to the square of the number density of O_2 (n_{O2}) at the surface. Therefore, the surface mixing ratio of BrO (i.e., between ground level and 300 m above ground level) is calculated according to:

$$X_{BrO,surf} = \frac{BrO^{dSCD}}{O_4^{dSCD}} \times \frac{n_{O2}^2}{n_{air}} \tag{5}$$

where dSCDs of BrO and O_4 (BrO^{dSCD} and O_4^{dSCD}, respectively) are collected by the MAX-DOAS instrument at the 2° elevation viewing angle and n_{air} is the density of air.

Hourly surface mixing ratios of BrO, calculated according to equation (5), are shown in Figure 3a. The error bars in Figure 3a are the 1σ uncertainty in the mixing ratio of BrO based on the root sum of squares combination of the BrO^{dSCD} error estimate and standard deviation about the daily mean. Based on the MAX-DOAS measurements at the 2° elevation angle, the mean and standard deviation of the surface mixing ratio of BrO over Fairbanks is 0.04 ± 0.29 ppt during the campaign. Additionally, for every day that daytime BrO^{VCD} is collected by MFDOAS (Figure 2), the values of surface BrO are within the fitting uncertainty of 0 ppt. This indicates that near-surface BrO does not have a significant impact on the OMI and MFDOAS retrievals of BrO^{VCD} shown in Figure 2.

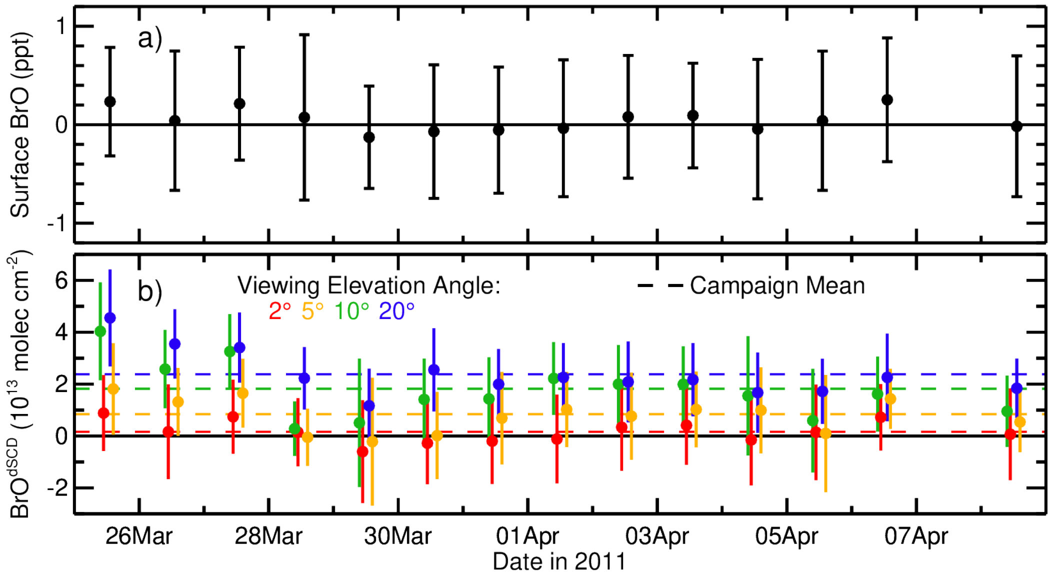

Figure 3. Daily mean cloud-cleared MAX-DOAS retrievals collected over Fairbanks, Alaska. (a) Points are daily mean surface mixing ratios of BrO, calculated according to equation 5. (b) Points are daily mean dSCD of BrO for four elevation angles (as indicated). Dashed lines are the campaign mean dSCD of BrO for four elevation angles. In both panels, error bars are the root sum of squares combination of the 1σ instrumental uncertainty and standard deviation about the daily mean.

Daily mean BrO^{dSCD}, retrieved by MAX-DOAS at 2, 5, 10, and 20° elevation angles are shown in Figure 3b. Error bars in Figure 3b are the root sum of squares combination of the 1σ fitting uncertainty and the standard deviation about the daily mean dSCD. The hourly timeseries for BrO^{dSCD} is shown in supporting information Figure S6, and campaign-averaged values of BrO^{dSCD} for each elevation angle are shown as dashed lines in Figure 3b and are listed in Table S2. For all days during the campaign, the BrO^{dSCD} retrieved by the 2° elevation angle (red in Figure 3b) is within uncertainty of zero, consistent with the results presented in Figure 3a. Daily mean values of BrO^{dSCD} are consistently positive throughout the campaign only at the 10 and 20° viewing elevation angles. Furthermore, the BrO^{dSCD} increase as the viewing elevation angle increases, indicating that over Fairbanks there is more BrO aloft than near the ground.

The relationship between BrO^{dSCD} and viewing elevation angle is investigated using the SCIATRAN (version 3.2.4) radiative transfer model (Rozanov et al., 2005). The SCIATRAN simulations are conducted considering gaseous O_3, BrO, NO_2, and O_4 absorbers and using a clean WMO aerosol profile with an albedo = 0.8 and aerosol optical depth = 0.07. AMFs, relative to the zenith, are simulated using SCIATRAN for each elevation angle with varying amounts of tropospheric BrO and assuming a stratospheric profile of BrO defined by the box model at local solar noon with JPL kinetics and 5 ppt of Br_y^{VSLS} (Section 2.3). Values of BrO^{dSCD} are calculated from each AMF, according to equation (3). Detailed results and a priori profiles of BrO considered in the radiative transfer study are presented in supporting information Figure S7.

The radiative transfer study indicates that tropospheric BrO is present aloft during the campaign. If the SCIATRAN model only considers a stratospheric profile of BrO, with no BrO below the tropopause, the simulated BrO^{dSCD} at the 20° elevation angle is 0.3×10^{13} molecules cm^{-2}. Even if the modeled value of Br_y^{VSLS} is increased from 5 to 9 ppt, the simulated BrO^{dSCD} is consistently lower than the retrievals of BrO^{dSCD} at the 20° elevation angle (blue in Figure 3b), indicating that BrO is present below the tropopause. Because larger values of BrO^{dSCD} were measured on 25 – 27 March than during the remainder of the campaign (Figure 3b), tropospheric mixing ratios of BrO are likely variable during the campaign.

For comparison to the tropospheric residual calculations presented in Section 3.4, we simulate BrO^{dSCD} using the same a priori profile used in equation (4) for interpreting tropospheric BrO from OMI retrievals. If the tropospheric mixing ratio of BrO is 2 ppt above 2 km, the SCIATRAN modeled value of BrO^{dSCD} is 2.1×10^{13} molecules cm^{-2} at the 20° viewing angle, in agreement with the MAX-DOAS campaign average at this viewing geometry (dotted blue line in Figure 3b). However, tropospheric BrO can be as low as 0.5 ppt above 2 km and the modeled BrO^{dSCD}, 0.8×10^{13} molecules cm^{-2} at 20°, is within uncertainty of the MAX-DOAS observations on 29 March and 4 April.

3.3. Interpreting the Stratospheric Column of BrO

In this section, we treat the total column measurements of BrO^{VCD} as purely stratospheric. Since the profile of tropospheric BrO is poorly constrained over Fairbanks, we first quantify the impact of stratospheric uncertainties on the interpretation of BrO^{VCD} retrievals. The stratospheric box model described in Section 2.3 is used to derive upper limits for Br_y^{VSLS} from OMI and MFDOAS retrievals of BrO^{VCD}. We quantify the sensitivity of the upper limit estimates of Br_y^{VSLS} to uncertainties in the retrievals and $BrONO_2$ kinetic parameters. In Section 3.4, we demonstrate how tropospheric BrO influences our interpretation of Br_y^{VSLS} and the retrievals of BrO^{VCD}.

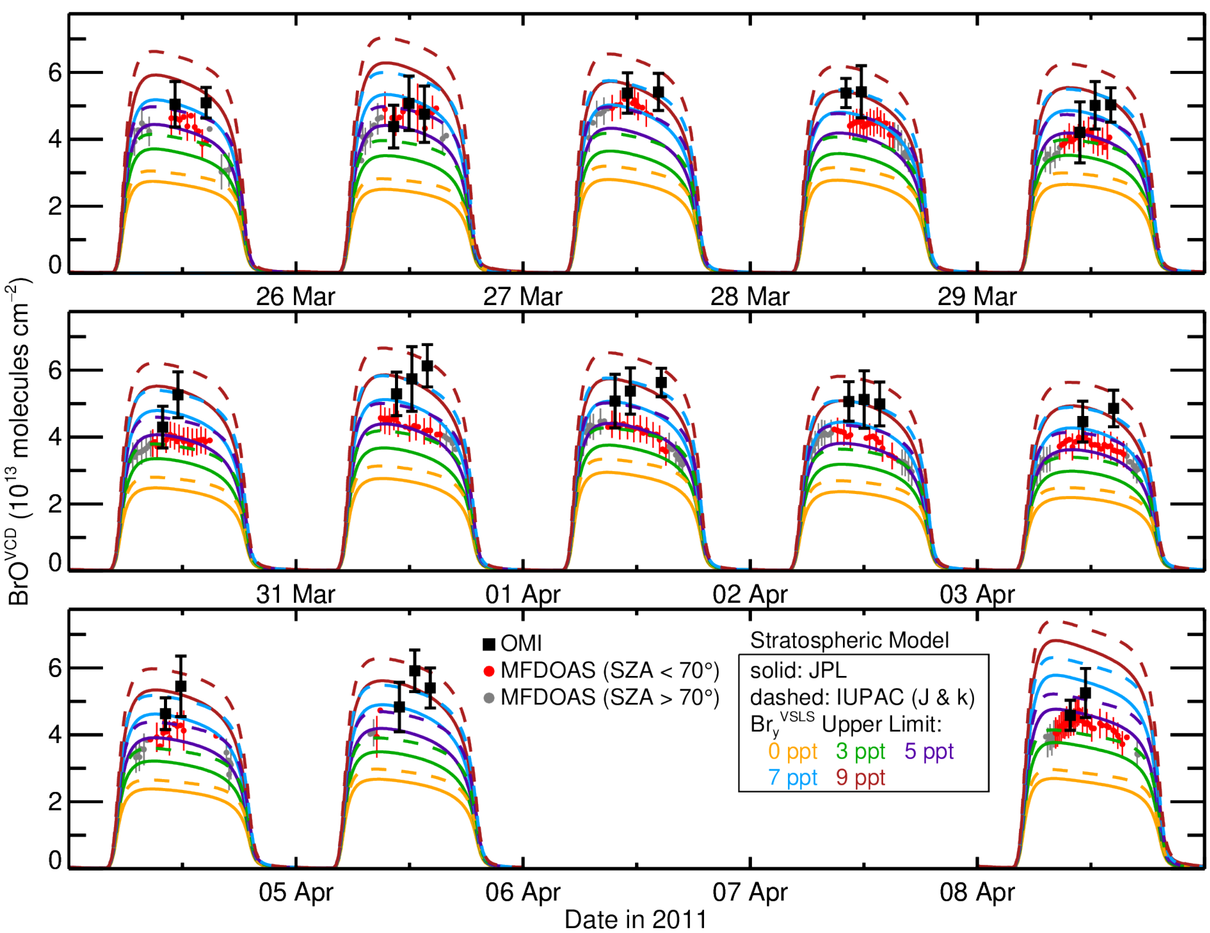

Figure 4. Retrievals of BrO^{VCD} and modeled stratospheric BrO^{VCD} over Fairbanks, Alaska during the 2011 campaign. Daytime observations of BrO^{VCD} are shown for MFDOAS in red and OMI in black. MFDOAS measurements of BrO^{VCD} collected at SZA > 70° are shown in grey. Error bars represent the 1σ total uncertainty in each measurement with error bars shown for every second MFDOAS measurement. Modeled stratospheric BrO^{VCD} is shown using solid lines for the JPL

kinetic scenario and using dashed lines for the IUPAC (J & k) scenario. Modeled stratospheric BrO^{VCD} is shown for five different loadings of Br_y^{VSLS} upper limits as indicated in the legend. Daytime MFDOAS measurements were not collected on 6 and 7 April.

For the entire spring 2011 campaign, vertical columns of stratospheric BrO are simulated with the box model using five kinetic scenarios: JPL, IUPAC (J), IUPAC (k), IUPAC (J & k), and Scaled (J & k), as described in Section 2.1.2. We focus first on a comparison of results using JPL and IUPAC (J & k) kinetics for five values of Br_y^{VSLS}. Figure 4 shows a comparison of measured BrO^{VCD} and modeled stratospheric BrO^{VCD} for all days where daytime MFDOAS measurements were collected during the campaign. In this figure, modeled values of stratospheric BrO^{VCD}, including five upper limit scenarios for Br_y^{VSLS}, are shown as solid lines for JPL kinetics and dashed lines for IUPAC (J & k) kinetics. The application of IUPAC parameters for $BrONO_2$ reactions increases the modeled BrO/Br_y ratio. As a result, smaller amounts of Br_y^{VSLS} need to be included in the model to simulate observations of BrO^{VCD} over Fairbanks.

The MFDOAS and OMI observations of BrO^{VCD} are shown in Figure 4 as a function of local solar time. MFDOAS observations of BrO^{VCD} collected during daytime (SZAs < 70°) are red, while MFDOAS observations collected in the morning and evening (SZA > 70°) are grey. Modeled stratospheric BrO^{VCD} gradually declines after solar noon. For most days during the campaign, the daytime MFDOAS observations (red points in Figure 4) generally follow the diurnal variation predicted by the stratospheric model, while the uncertainties in the MFDOAS and OMI retrievals typically encompass the modeled diurnal variation.

Our stratospheric model (Section 2.3) is constrained to GMI output at the OMI overpass time as well as OMI and ozonesonde measurements. In our simulations of BrO^{VCD}, we assume stratospheric Br_y, O_3, and NO_y are constant throughout the day. During the campaign, the OMI overpass time is close to solar noon, while the ozonesondes were launched near 11:00 local solar time. The effect of atmospheric transport could potentially mean that the ozone measurements and CFC-11 output from GMI, used to define stratospheric Br_y, may not be representative of the entire 24 hour period. The potential impact of diurnal changes in atmospheric dynamics on our calculation of Br_y^{VSLS} upper limits is explored in Section 3.3.2.

At SZAs larger than ~70°, model BrO^{VCD} deviate from the daytime linear trend. In the twilight hours, BrO^{VCD} changes rapidly with time. The detailed shape of the morning rise and evening decay is sensitive to uncertainties in k_1 and J_2 (Kreycy et al., 2013). However, due to uncertainties in the tropospheric loading of BrO (Section 3.1) as well as atmospheric transport during the day, we are not able to conclusively evaluate the kinetic adjustments proposed by Kreycy et al. (2013) using MFDOAS twilight observations.

To clearly depict the difference between the JPL and IUPAC (J & k) kinetic scenarios, the observed BrO^{VCD} and modeled stratospheric BrO^{VCD} for the whole campaign is shown at noon in Figure 5. In this figure, MFDOAS and OMI daytime BrO^{VCD} are scaled to noon using the modeled diurnal variation, shown in Figure 4. This scaling is conducted by calculating the ratio of modeled BrO^{VCD} at 12:00 local solar time to BrO^{VCD} at the time of each observation. Daytime MFDOAS and OMI measurements of BrO^{VCD} are multiplied by this modeled ratio to scale each observation to noon. The noon-normalized daily mean for each set of measurements is shown in Figure 5, where the error bars are the combination in quadrature of the standard deviation about the mean and the 1σ instrumental uncertainty. Dotted lines are modeled BrO^{VCD} at noon for the JPL (Figure 5a) and IUPAC (J & k) (Figure 5b) simulations with 0 to 9 ppt of Br_y^{VSLS} (in 2 ppt increments).

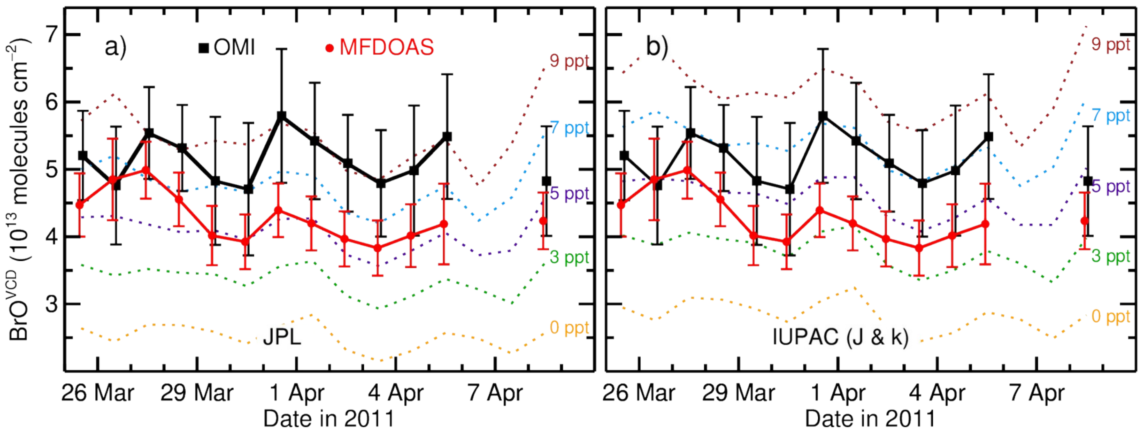

Figure 5. Measured BrO^{VCD} and modeled stratospheric BrO^{VCD} over Fairbanks, Alaska for all days of the spring 2011 campaign. Points are daily mean measurements, scaled to noon using modeled diurnal variation of stratospheric BrO^{VCD}, and error bars are combination of the standard deviation about the daily mean and the 1σ measurement uncertainty. Dotted lines are modeled stratospheric BrO^{VCD} at noon using (a) JPL kinetics and (b) IUPAC (J & k) kinetics for various values of upper limit Br_y^{VSLS}, ranging from 0 to 9 ppt.

3.3.1. Defining Upper Limits on the Contribution of VSLS to Stratospheric Bromine

In Figure 5a and the solid lines in Figure 4, stratospheric BrO^{VCD} is modeled using JPL kinetics. If these simulations include 5 ppt of Br_y^{VSLS}, the modeled stratosphere closely represents MFDOAS measurements on most days in March and April 2011, except for 26 – 28 March where larger amounts of Br_y^{VSLS} are needed to fully account for the retrievals. The JPL simulations generally need to include between 7 and 9 ppt of Br_y^{VSLS} to simulate OMI observations of BrO^{VCD} without including tropospheric BrO.

Table 2. Mean estimates for the upper limit of Br_y^{VSLS} based on OMI and MFDOAS observations of BrO^{VCD} for five kinetic scenarios.

Instrument	Br_y^{VSLS} (ppt)				
	JPL	IUPAC (J)	IUPAC (k)	IUPAC (J & k)	Scaled (J & k)
OMI	8.0 ± 2.6	7.6 ± 2.5	6.5 ± 2.3	6.2 ± 2.2	6.2 ± 2.2
MFDOAS	5.3 ± 1.5	4.9 ± 1.4	4.1 ± 1.3	3.8 ± 1.3	3.8 ± 1.2

To determine upper limits of Br_y^{VSLS}, we interpolate simulations of BrO^{VCD} as a function of Br_y^{VSLS} to the value of each daytime OMI and MFDOAS measurement shown in Figure 4. The mean values of the upper limits on Br_y^{VSLS} are given in Table 2 for both OMI and MFDOAS as well as five kinetic scenarios. The uncertainty reported in Table 2 is the combination in quadrature of the standard deviation about the mean interpolated value of Br_y^{VSLS} as well as the uncertainty in Br_y^{VSLS} due to measurement uncertainties of BrO^{VCD} and the OMI stratospheric column NO_2. The uncertainty in our upper limit estimates of Br_y^{VSLS} is described in further detail in Section 3.3.2.

The WMO 2018 Ozone Assessment recommends a value of 5 ± 2 ppt for Br_y^{VSLS}. The recommended value is based on aircraft observations collected in the tropics (Engel et al., 2018). If the stratosphere is simulated using JPL kinetics, the OMI-based upper limit for Br_y^{VSLS} is 8.0 ± 2.6 ppt, above the WMO 2018 range and supporting the presence of tropospheric BrO over Fairbanks. The MFDOAS and JPL-based upper limit for Br_y^{VSLS} is 5.3 ± 1.1 ppt and is in close agreement with the WMO central value only if the tropospheric column of BrO is not significant over Fairbanks for the majority of the campaign, except for 26 – 28 March where the 5 ppt Br_y^{VSLS} scenario underestimates MFDOAS BrO^{VCD} (Figures 4 and 5a).

In Figure 5b and the dashed lines in Figure 4, stratospheric BrO^{VCD} is modeled using the IUPAC kinetic parameters for $BrONO_2$ formation (reaction 1) and photolysis (reaction 2). For this kinetic scenario, the upper limit of Br_y^{VSLS} is 6.2 ± 2.2 ppt based on OMI retrievals and 3.8 ± 0.9 ppt based on MFDOAS. The WMO 2018 value for Br_y^{VSLS} is expected to be less sensitive to uncertainties in $BrONO_2$ kinetics than observed over Fairbanks since a smaller fraction of Br_y is in the form of $BrONO_2$ in air crossing the tropopause (Liang et al., 2014; Wales et al., 2018). Thus, the OMI-based upper limit of Br_y^{VSLS} is well within the upper limit of the WMO recommendations for the IUPAC (J & k) simulations, while the MFDOAS-based upper limit with the IUPAC (J & k) kinetics would restrict the potential value of Br_y^{VSLS} to the lower (5 to 3 ppt) limit of the WMO range.

The IUPAC (J & k) simulations are in close agreement with the Scaled (J & k) modeled runs, which follow the kinetic adjustments suggested by Kreycy et al. (2013). The IUPAC (J) scenario uses only the $BrONO_2$ cross sections from IUPAC, and the IUPAC (k) scenario uses only the reaction (1) rate constant from IUPAC with all other kinetic parameters following JPL. More than half of the decrease between the estimates of Br_y^{VSLS} for the JPL and IUPAC (J & k) simulations is due to the different kinetic recommendations for reaction (1), as demonstrated by the IUPAC (k) scenario (Table 2).

3.3.2. Error Analysis

Here we assess the uncertainties that impact our upper limit estimates of Br_y^{VSLS}. The absolute error reported in Table 2 includes uncertainties due to the following factors: the measurement uncertainty in each retrieval of BrO^{VCD}, the measurement uncertainty in the OMI stratospheric column NO_2 used to constrain the box model, and the standard deviation about the mean upper limit estimate of Br_y^{VSLS}.

On average, the 1σ measurement uncertainty contributes a relative error of 24% for MFDOAS and 26% for OMI-based upper limit estimates of Br_y^{VSLS} given in Table 3. This was determined by interpolating modeled stratospheric BrO^{VCD} as a function of Br_y^{VSLS} to the upper and lower 1σ uncertainty of each observation of BrO^{VCD} shown in Figure 4. Additionally, the modeled BrO/Br_y ratio is sensitive to the value of NO_2 used in the photochemical box model. We determine that the $\pm 2 \times 10^{14}$ molecules cm^{-2} uncertainty in OMI stratospheric column NO_2 contributes a minor, ~0.2 ppt, to all uncertainties of Br_y^{VSLS} upper limits in Table 2 by repeating simulations of BrO^{VCD} constrained to match the upper and lower limit uncertainties in stratospheric NO_2.

The standard deviation about the mean upper limit value of Br_y^{VSLS} is 19% and 22% respectively for MFDOAS and OMI-based estimates. The variation of the observations about the modeled stratospheric column BrO^{VCD} for a given Br_y^{VSLS} scenario is likely due to changes in tropospheric BrO during the campaign (Section 3.2) and diurnal stratospheric transport not accounted for in the box model.

As discussed with Figure 4, the box model is constrained to a single profile of Br_y per day, defined by midday observations and GMI output (Section 2.3). This method does not account for stratospheric transport that could alter the stratospheric Br_y profile during the day. We use vertical column densities of O_3 (O_3^{VCD}) as an indicator for possible changes in atmospheric dynamics. In general, we expect that O_3^{VCD} and stratospheric Br_y are positively correlated with each other (e.g, Theys et al., 2009). Values of O_3^{VCD} over Fairbanks are shown in Figure S8 of the supporting information for 25 March through 8 April. Observations of O_3^{VCD} from OMI and the ground-based Brewer spectrometer (Tzortziou et al., 2012) are included in Figure S8 as well as simulations from the National Center for Environmental Prediction (NCEP; doi: 10.5065/D6M043C6). For example, large decreases in O_3^{VCD} are observed during the day on 1 and 2 April, and a large increase in O_3^{VCD} is simulated by the NCEP-final model on 4 April. Consequently, our assumption of a single stratospheric profile of Br_y throughout the day may not be valid on these three days. While the diurnal variation in MFDOAS BrO^{VCD} is well captured by the model on 1 April, decreases and increases in MFDOAS BrO^{VCD} on 2 April and 4 April, respectively, do not follow the modeled diurnal variation (Figure 4).

3.4. Tropospheric Residual BrO

Based on MAX-DOAS observations, BrO is not present near the surface (i.e., below 300 m) over Fairbanks during the campaign (Figure 3a). However, MAX-DOAS retrievals at larger viewing elevation angles above the horizon suggest that tropospheric BrO is present aloft during the campaign, and Br_y compounds could be transported to the troposphere from the stratosphere or from either non-local tropospheric sources. Because the MAX-DOAS instrument is not able to accurately quantify tropospheric BrO that is located over ~2 km above the surface, we estimate tropospheric BrO during the campaign using the retrievals of BrO^{VCD} and the stratospheric model. Past studies have estimated that the tropospheric background BrO^{VCD} can range from below 1×10^{13} molecules cm^{-2} (Schofield et al., 2004, 2006) to up to 3×10^{13} molecules cm^{-2} (Theys et al., 2011; Van Roozendael et al., 2002). Here, we assess the sensitivity of calculations for residual tropospheric BrO to the uncertainties in Br_y^{VSLS}, $BrONO_2$ kinetics, and the two different datasets of BrO^{VCD}.

Our interpretation of the OMI-based tropospheric residual column is dependent on the chosen a priori profile used in equation (4), but an observationally constrained profile is not available from the MAX-DOAS data. In general, profile information for BrO in the Arctic troposphere is limited. Previous aircraft studies that sampled the Arctic upper troposphere reported mixing ratios of BrO at or near the 1.5 and 2 ppt lower limit of detection of their instruments (Neuman et al., 2010; Prados-Roman et al., 2011). For simplicity, the OMI values of tropospheric BrO are calculated according to Section 2.4 assuming a tropospheric profile of BrO with no BrO below 2km and a constant mixing ratio of BrO between 2 km and the tropopause, above the altitude sensitivity of the MAX-DOAS instrument. The MFDOAS retrievals of BrO^{VCD} involve a nearly geometric AMF that has a weak dependence on profile shape for SZAs < 75°. Thus, we calculate tropospheric BrO from MFDOAS as the difference between the total retrieved and modeled stratospheric BrO^{VCD}.

In Table 3, tropospheric column BrO is calculated from OMI and MFDOAS retrievals of BrO^{VCD} using modeled stratospheric BrO^{VCD} (Section 2.3). The second and third columns of Table 3 respectively indicate the kinetic scenario and value of Br_y^{VSLS} used to model stratospheric BrO^{VCD}. The values of Br_y^{VSLS} included in the stratosphere were chosen to represent the WMO 2018 5 ± 2 ppt best estimate from studies based in the tropics. The tropospheric mixing ratio of BrO is calculated from tropospheric BrO^{VCD} assuming that BrO is vertically mixed between 2 km and the tropopause height. The reported tropospheric BrO values are the mean and standard deviation during the Fairbanks campaign.

Table 3. Mean and standard deviation of calculated tropospheric BrO.

Instrument	Model Setup		Tropospheric BrO	
	Kinetics	Br_y^{VSLS} (ppt)	Column (10^{13} molecules cm^{-2})	Mixing Ratio[a] (ppt)
OMI	JPL	7	0.4 ± 1.0	0.4 ± 1.0
OMI	JPL	5	1.5 ± 0.8	1.4 ± 0.8
OMI	JPL	3	2.6 ± 0.7	2.5 ± 0.6
OMI	IUPAC (J & k)	5	0.7 ± 0.8	0.6 ± 0.8
MFDOAS	JPL	5	0.1 ± 0.3	0.1 ± 0.4
MFDOAS	JPL	3	0.8 ± 0.3	0.8 ± 0.3

[a]Assuming BrO is well mixed between 2 km and the tropopause

The first three rows in Table 3 utilize OMI measurements of BrO^{VCD} and stratospheric simulations with JPL kinetics. When stratospheric BrO^{VCD} is simulated using JPL kinetics and the WMO 2018 central, 5 ppt estimate of Br_y^{VSLS}, we calculate a tropospheric residual of 1.5 ± 0.8 × 10^{13} molecules cm^{-2}, and a tropospheric mixing ratio of 1.4 ± 0.8 ppt, which is well within the uncertainty of the MAX-DOAS observations at larger viewing angles (Section 3.2).

Our calculated tropospheric column is sensitive to the assumed profile shape of tropospheric BrO. In general, the satellite retrieval is less sensitive to BrO that is located closer to the ground than higher in altitude. For example, if we assume a tropospheric profile of BrO that increases linearly from 1 km to the tropopause height (i.e., the green line in Figure S7a), our

OMI-based tropospheric column, calculated using JPL kinetics and 5 ppt of Br_y^{VSLS} in the stratosphere, decreases slightly to 1.4×10^{13} molecules cm^{-2}. If we assume a tropospheric profile that decreases linearly from 1 km to the tropopause height, this column increases to 2.3×10^{13} molecules cm^{-2}.

The range in Br_y^{VSLS} is the largest source of uncertainty in our calculation of tropospheric residual BrO^{VCD} over Fairbanks. The OMI-based tropospheric residual BrO ranges from 0.4 to 2.6×10^{13} molecules cm^{-2} over Fairbanks based on the 7 to 3 ppt uncertainty in Br_y^{VSLS}, respectively. Only if the WMO 2018 lower limit for Br_y^{VSLS} (i.e., 3 ppt) is applied do we find evidence for background tropospheric BrO^{VCD} close to the 3×10^{13} molecules cm^{-2} upper limit proposed by previous satellite-based studies (Theys et al., 2011; Van Roozendael et al., 2002). If the stratospheric model does not account for Br_y^{VSLS} (i.e., Br_y^{VSLS} = 0 ppt), the calculated tropospheric residual would increase to $3.9 \pm 0.7 \times 10^{13}$ molecules cm^{-2}, further demonstrating the importance of accurately representing the stratospheric bromine burden.

The IUPAC parameters for $BrONO_2$ kinetics increase the simulated ratio of BrO/Br_y. If we model stratospheric BrO^{VCD} using IUPAC (J & k) kinetics and 5 ppt of Br_y^{VSLS}, we calculate tropospheric BrO^{VCD} is $0.7 \pm 0.8 \times 10^{13}$ molecules cm^{-2} over Fairbanks based on OMI measurements. This value is 0.8×10^{13} molecules cm^{-2} lower than OMI-based calculations using JPL kinetics and is the smallest uncertainty in our calculation of tropospheric residual BrO.

The second largest uncertainty in our calculation of tropospheric BrO^{VCD} is due to the difference between OMI and MFDOAS retrievals of BrO^{VCD}. Our calculation of tropospheric BrO^{VCD} is $0.1 \pm 0.3 \times 10^{13}$ molecules cm^{-2} based on MFDOAS retrievals and stratospheric BrO^{VCD} simulated using JPL kinetics and 5 ppt of Br_y^{VSLS}. Consequently, the MFDOAS retrievals and the

5 ppt best estimate of Br_y^{VSLS} suggest that tropospheric BrO is not continuously present during the Fairbanks campaign, which is not supported by the MAX-DOAS observations (Section 3.2).

If the box model uses JPL kinetics and the lower, 3 ppt, limit of the WMO estimate of Br_y^{VSLS}, the mean value of tropospheric BrO is 0.8×10^{13} molecules cm^{-2} based on MFDOAS (last row of Table 3). The campaign mean, 0.8 ppt, value of tropospheric BrO is near the lower limit of uncertainty of the MAX-DOAS radiative transfer analysis (Figure S7). For this stratospheric scenario, the daily mean tropospheric column BrO is the difference between MFDOAS BrO^{VCD} in Figure 5a and the dotted green line (i.e., stratospheric column BrO with JPL kinetics and 3 ppt of Br_y^{VSLS}). The daily mean tropospheric residual BrO is above 1×10^{13} molecules cm^{-2} on 26 – 28 March, while the MAX-DOAS observations of BrO^{dSCD} in the 20° viewing geometry are larger on 25 – 27 March than during the rest of the 2011 campaign (Figure 3b). This provides support for daily variability in tropospheric BrO over Fairbanks.

4. Conclusions

In this study, we compare ground-based retrievals of vertical column density of BrO (BrO^{VCD}) collected over Fairbanks, Alaska in March and April 2011 to retrievals of BrO^{VCD} obtained by the OMI instrument onboard the NASA Aura satellite. Our analysis is based on version 3.0.5 of the OMI retrieval of BrO^{VCD} (Suleiman et al., 2019) and ground-based observations of BrO^{VCD} from the Washington State University multifunction DOAS (MFDOAS) instrument (Herman et al., 2009; Spinei et al., 2010). Due to their impact on stratospheric ozone, there is widespread interest in quantifying the role of biogenic, brominated very short-lived substances (VSLS) on the stratospheric bromine burden. Similarly, in the troposphere reactive bromine compounds reduce levels of ozone and alter the oxidative capacity (Saiz-Lopez & von Glasow, 2012; Simpson et al., 2015). Since the magnitude of the contribution of VSLS to stratospheric bromine (Br_y^{VSLS}) is the largest uncertainty in the stratospheric burden of bromine, accurate interpretations of BrO^{VCD} require a precise understanding of Br_y^{VSLS}. The primary goal of this study is to constrain upper limits for Br_y^{VSLS}, and the secondary goal is to evaluate the relative contributions of BrO from the stratosphere and the troposphere to total BrO^{VCD}.

Fairbanks is located in central Alaska and is isolated from wind-blown sea salt and marine sources of inorganic bromine. During the campaign, the University of Alaska multi-axis DOAS (MAX-DOAS) instrument detected no BrO near the surface over Fairbanks. However, MAX-DOAS scans at higher (i.e., 10 and 20°) elevation angles above the horizon suggest the presence of tropospheric BrO aloft during the campaign. Because the slant path length through the troposphere decreases as the MAX-DOAS elevation angle increases, profile information is not available for tropospheric BrO over Fairbanks. Thus, we first calculate upper limits for Br_y^{VSLS} and quantify stratospheric sources of uncertainty by treating the OMI and MFDOAS measurements of BrO^{VCD} as purely stratospheric.

We calculate a range of 4 to 8 ppt for the upper limit of Br_y^{VSLS} using a stratospheric model and ground and satellite-based retrievals of BrO^{VCD}. In comparison, the 2018 WMO Ozone Assessment (WMO 2018) estimate for Br_y^{VSLS} is 5 ± 2 ppt based on observations of VSLS and BrO entering the stratosphere through the tropical tropopause layer (Engel et al., 2018), and past estimates for Br_y^{VSLS} based on stratospherically aged air range from 3 to 9 ppt (Montzka et al., 2011). The difference between the ground and satellite-based retrievals of BrO^{VCD} is the largest source of uncertainty in our evaluation of Br_y^{VSLS}, presenting a 2.6 ppt uncertainty in our upper limit estimate. Uncertainties in kinetic parameters governing the daytime partitioning of $BrONO_2$ via reactions (1) and (2) contribute an additional 1.7 ppt uncertainty in our evaluation of Br_y^{VSLS}.

The OMI measurements of BrO^{VCD} over Fairbanks are typically higher than MFDOAS observations with a relative bias of 20 ± 14%. The magnitude of BrO^{VCD} is highly sensitive to the choice of the spectral fitting window used in the retrieval (Aliwell et al., 2002; Seo et al., 2018; Vogel et al., 2013), as demonstrated for both MFDOAS in this study and OMI in previous studies (Suleiman et al., 2019). Each retrieval used a fitting window optimized for that instrument: the OMI window is 319 to 347 nm and MFDOAS is 336 to 359 nm. If we estimate upper limits for Br_y^{VSLS} with a stratospheric model using kinetic parameters recommended by the JPL kinetic evaluation (Burkholder et al., 2015), 8.0 ± 2.5 ppt of Br_y^{VSLS} must be included in the model to simulate OMI satellite-based measurements of BrO^{VCD}, which is slightly larger than the 7 ppt upper limit of the WMO 2018 estimate, suggesting the presence of tropospheric BrO. However, only 5.3 ± 1.1 ppt of Br_y^{VSLS} is needed to represent MFDOAS ground based BrO^{VCD}, which is in agreement with the WMO 2018 estimate only if tropospheric BrO is not ubiquitous over Fairbanks during the campaign.

Our interpretation of Br_y^{VSLS} from measurements of BrO^{VCD} is further complicated by uncertainties in the kinetics that govern the formation and loss of $BrONO_2$. The JPL (Burkholder et al., 2015) and IUPAC (Atkinson et al., 2007) kinetic evaluations review the same laboratory studies for the termolecular formation of $BrONO_2$ (reaction 1) and $BrONO_2$ photolysis (reaction 2), but the two evaluations propose different rate constants and absorption cross sections for these two reactions. At stratospheric temperatures, the IUPAC parameters result in faster formation of $BrONO_2$ and slower $BrONO_2$ photolysis than the JPL recommendations, similar to kinetic adjustments proposed by Kreycy et al. (2013). As a result, smaller quantities of Br_y^{VSLS} are needed to model observed values of BrO^{VCD} when IUPAC $BrONO_2$ kinetics are applied. The uncertainty in reaction (1) accounts for ~80% of the difference between JPL and IUPAC-based upper limit estimates of Br_y^{VSLS}. Consequently, if future laboratory studies support a slower rate constant for the formation of $BrONO_2$ (reaction 1) at stratospherically relevant temperatures, previous estimates for Br_y^{VSLS} based on observations of BrO in stratospherically aged air could be reduced by ~1.4 ppt.

We evaluate the potential influence of tropospheric BrO on our interpretation of retrievals of BrO^{VCD}. The OMI-based tropospheric residuals are determined with modeled stratospheric BrO^{VCD} and tropospheric air mass factors calculated according to Choi et al. (2012). If we assume the WMO 2018 best estimate of Br_y^{VSLS} (5 ppt) as well as JPL kinetics in the stratospheric model, the mean and standard deviation of tropospheric BrO^{VCD} over Fairbanks is found to be $1.5 \pm 0.8 \times 10^{13}$ molecules cm^{-2}. In this case, tropospheric BrO would result from either long-range transport of surface emissions or stratosphere to troposphere exchange. This value for tropospheric BrO is supported by analysis of MAX-DOAS observations using a radiative transfer model, is in agreement with ground-based tropospheric column retrievals collected over Harestua, Norway (60°N; Hendrick et al., 2007), and is near the lower limit of previous estimates for background tropospheric BrO (Theys et al., 2011; Van Roozendael et al., 2002). Therefore, agreement between the WMO 2018 best estimate of Br_y^{VSLS}, OMI retrievals of BrO^{VCD}, and MAX-DOAS monitoring of tropospheric BrO can be achieved without application of kinetic adjustments to $BrONO_2$ kinetics.

If we assume 5 ppt of Br_y^{VSLS} and JPL kinetics in the stratosphere, the MFDOAS retrieval of BrO^{VCD} indicates tropospheric BrO^{VCD} is $0.1 \pm 0.3 \times 10^{13}$ molecules cm^{-2} during the campaign. This value suggests that tropospheric BrO is not present over Fairbanks for most days during the campaign, which is not supported by our interpretation of the MAX-DOAS data. Thus, the 3 ppt lower limit for the WMO 2018 estimate of Br_y^{VSLS} is needed to bring MFDOAS-based tropospheric residual of BrO within uncertainty of the MAX-DOAS observations of tropospheric residual BrO. Additionally, both the MAX-DOAS scans at higher elevation angles and the MFDOAS-based tropospheric residual BrO indicate that the magnitude of tropospheric BrO is variable during the campaign.

Finally, we quantify stratospheric sources of uncertainty in the OMI-based tropospheric residual BrO. The 3 to 7 ppt range in the WMO 2018 recommendation for Br_y^{VSLS} places a $\pm 1.0 \times 10^{13}$ molecules cm^{-2} uncertainty on our estimate of tropospheric residual BrO. Consequently, the uncertainty in the stratospheric bromine burden is the largest source of uncertainty in our tropospheric residual calculation. Uncertainties in the retrieval of BrO^{VCD} contribute additional uncertainties to the calculation of tropospheric residual BrO, and the $BrONO_2$ kinetic parameters are the smallest source of uncertainty in our calculation of tropospheric residual BrO over Fairbanks.

Acknowledgments

PAW, RJS, and TPC appreciate support from the NASA Atmospheric Composition Modeling and Analysis Program (ACMAP) and the Aura Science Team for this research, under NASA grants NNX17AH05G and 80NSSC19K0983. The MFDOAS instrument deployment was supported by NASA grant NNX09AJ28G. Part of the research was carried out at the Jet Propulsion Laboratory, California Institute of Technology, under contract with NASA. Research at the Smithsonian Astrophysical Observatory was supported by NASA. OMI data are available at NASA Goddard Earth Sciences Data and Information Services Center (GES DISC; https://disc.gsfc.nasa.gov/), and the Fairbanks 2011 campaign data are available at the Aura Validation Data Center (AVDC; https://avdc.gsfc.nasa.gov/). We thank all reviewers for numerous helpful comments that lead to a substantial improvement of the submitted manuscript.

References

Aliwell, S. R., Van Roozendael, M., Johnston, P. V., Richter, A., et al. (2002). Analysis for BrO in zenith-sky spectra: An intercomparison exercise for analysis improvement. *J. Geophys. Res. Atmos.*, *107*(14), 1–20. doi: 10.1029/2001JD000329

Aschmann, J., Sinnhuber, B. M., Atlas, E. L., & Schauffler, S. M. (2009). Modeling the transport of very short-lived substances into the tropical upper troposphere and lower stratosphere. *Atmos. Chem. Phys.*, *9*(23), 9237–9247. doi: 10.5194/acp-9-9237-2009

Atkinson, R., Baulch, D. L., Cox, R. a., Crowley, J. N., et al. (2007). Evaluated kinetic and photochemical data for atmospheric chemistry: Volume III -- gas phase reactions of inorganic halogens. *Atmos. Chem. Phys.*, *7*, 981–1191. doi: 10.5194/acp-6-3625-2006

Barrie, L. A., Bottenheim, J. W., Schnell, R. C., Crutzen, P. J., & Rasmussen, R. A. (1988). Ozone destruction and photochemical reactions at polar sunrise in the lower Arctic atmosphere. *Nature*, *334*(6178), 138–141. doi: 10.1038/334138a0

Brion, J., Chakir, A., Daumont, D., Malicet, J., & Parisse, C. (1993). High-resolution laboratory absorption cross section of O_3. Temperature effect. *Chem. Phys. Lett.*, *213*(5–6), 610–612. doi: 10.1016/0009-2614(93)89169-I

Bucsela, E. J., Krotkov, N. A., Celarier, E. A., Lamsal, L. N., et al. (2013). A new stratospheric and tropospheric NO_2 retrieval algorithm for nadir-viewing satellite instruments: applications to OMI. *Atmos. Meas. Tech.*, *6*(10), 2607–2626. doi: 10.5194/amt-6-2607-2013

Burkholder, J. B., Ravishankara, A. R., & Solomon, S. (1995). UV/visible and IR absorption cross sections of $BrONO_2$. *J. Geophys. Res.*, *100*(D8), 16793. doi: 10.1029/95JD01223

Burkholder, J. B., Sander, S. P., Abbatt, J., Barker, J. R., et al. (2015). *Chemical Kinetics and Photochemical Data for Use in Atmospheric Studies, Evaluation Number 18. JPL Publication 15-10*. Jet Propulsion Laboratory, Pasadena. Retrieved from http://jpldataeval.jpl.nasa.gov/

Chen, D., Huey, L. G., Tanner, D. J., Salawitch, R. J., et al. (2016). Airborne measurements of BrO and the sum of HOBr and Br_2 over the Tropical West Pacific from 1 to 15 km during the CONvective TRansport of Active Species in the Tropics (CONTRAST) experiment. *J. Geophys. Res. Atmos.*, *121*(20), 12,560-12,578. doi: 10.1002/2016JD025561

Choi, S., Theys, N., Salawitch, R. J., Wales, P. A., et al. (2018). Link Between Arctic Tropospheric BrO Explosion Observed From Space and Sea-Salt Aerosols From Blowing Snow Investigated Using Ozone Monitoring Instrument BrO Data and GEOS-5 Data Assimilation System. *J. Geophys. Res. Atmos.*, *123*(13), 6954–6983. doi: 10.1029/2017JD026889

Choi, S., Wang, Y., Salawitch, R. J., Canty, T., et al. (2012). Analysis of satellite-derived Arctic tropospheric BrO columns in conjunction with aircraft measurements during ARCTAS and ARCPAC. *Atmos. Chem. Phys.*, *12*(3), 1255–1285. doi: 10.5194/acp-12-1255-2012

Danis, F., Caralp, F., Masanet, J., & Lesclaux, R. (1990). Kinetics of the Reaction BrO+ NO_2+ M $\rightarrow$ $BrONO_2$ + M in the Temperature Range 263-343 K. *Chem. Phys. Lett.*, *167*(5), 450–456.

Deters, B., Burrows, J. P., & Orphal, J. (1998). UV-visible absorption cross sections of bromine nitrate determined by photolysis of $BrONO_2$/Br2 mixtures. *J. Geophys. Res.*, *103*(D3), 3563–3570.

Dorf, M., Butz, A., Camy-Peyret, C., Chipperfield, M. P., et al. (2008). Bromine in the tropical troposphere and stratosphere as derived from balloon-borne BrO observations. *Atmos.*

Chem. Phys., *8*(23), 7265–7271. doi: 10.5194/acp-8-7265-2008

Engel, A., Rigby, M., Burkholder, J. B., Fernandez, R. P., et al. (2018). Update on Ozone-Depleting Substances (ODSs) and Other Gases of Interest to the Montreal Protocol, Chapter 1. In *Scientific Assessment of Ozone Depletion: 2018, Global Ozone Research and Monitoring Project – Report No. 58*. Geneva, Switzerland: World Meteorological Organization.

Engel, A., Strunk, M., Müller, M., Haase, H.-P., et al. (2002). Temporal development of total chlorine in the high-latitude stratosphere based on reference distributions of mean age derived from CO2 and SF6. *J. Geophys. Res*, *107*(12), ACH 1-1-ACH 1-11. doi: 10.1029/2001JD000584

Eyring, V., Lamarque, J.-F., Hess, P., Arfeuille, F., et al. (2013). Overview of IGAC/SPARC Chemistry-Climate Model Initiative (CCMI) community simulations in support of upcoming ozone and climate assessments. *SPARC Newsl.*, *40*, 48–66. Retrieved from http://www.sparc-climate.org/fileadmin/customer/6_Publications/Newsletter_PDF/40_SPARCnewsletter_Jan2013_web.pdf

Frieß, U., Sihler, H., Sander, R., Pöhler, D., et al. (2011). The vertical distribution of BrO and aerosols in the Arctic: Measurements by active and passive differential optical absorption spectroscopy. *J. Geophys. Res.*, *116*(18), D00R04. doi: 10.1029/2011JD015938

Hendrick, F., Van Roozendael, M., Chipperfield, M. P., Dorf, M., et al. (2007). Retrieval of stratospheric and tropospheric BrO profiles and columns using ground-based zenith-sky DOAS observations at Harestua, 60°N. *Atmos. Chem. Phys. Discuss.*, *7*(3), 8663–8708. doi: 10.5194/acpd-7-8663-2007

Herman, J., Cede, A., Spinei, E., Mount, G., et al. (2009). NO_2 column amounts from ground-based Pandora and MFDOAS spectrometers using the direct-sun DOAS technique: Intercomparisons and application to OMI validation. *J. Geophys. Res. Atmos.*, *114*(13), 1–20. doi: 10.1029Z2009JD011848

Hermans, C., Vandaele, A. C., Carleer, M., Fally, S., et al. (1999). Absorption cross-sections of atmospheric constituents: NO_2, O_2, and H_2O. *Environ. Sci. Pollut. Res.*, *6*(3), 151–158. doi: 10.1007/BF02987620

Honninger, G., & Platt, U. (2002). Observations of BrO and its vertical distribution during surface ozone depletion at Alert. *Atmos. Environ.*, *36*(15–16), 2481–2489.

Johnson, B. J., Cullis, P. D., & ESRL, N. (2018). Earth System Research Laboratory Ozone Water Vapor Group Ozonesonde Measurments, Version 1. doi: 10.7289/V5CC0XZ1

Klobas, J. E., Wilmouth, D. M., Weisenstein, D. K., Anderson, J. G., & Salawitch, R. J. (2017). Ozone depletion following future volcanic eruptions. *Geophys. Res. Lett.* doi: 10.1002/2017GL073972

Ko, M. K. W., Poulet, G., Blake, D. R., Boucher, O., et al. (2003). Very short-lived halogen and sulfur substances, Chapter 2. In *Scientific Assessment of Ozone Depletion: 2002, Global Ozone Research and Monitoring Project – Report No. 47*. Geneva, Switzerland: World Meteorological Organization.

Koenig, T. K., Volkamer, R., Baidar, S., Dix, B., et al. (2017). BrO and inferred Bry profiles over the western Pacific: relevance of inorganic bromine sources and a Bry minimum in the aged tropical tropopause layer. *Atmos. Chem. Phys.*, *17*(24), 15245–15270. doi: 10.5194/acp-17-15245-2017

Kovalenko, L. J., Livesey, N. L., Salawitch, R. J., Camy-Peyret, C., et al. (2007). Validation of Aura Microwave Limb Sounder BrO observations in the stratosphere. *J. Geophys. Res.*

Atmos., *112*(24), 1–17. doi: 10.1029/2007JD008817

Kreycy, S., Camy-Peyret, C., Chipperfield, M. P., Dorf, M., et al. (2013). Atmospheric test of the $J(BrONO_2)/k_{BrO+NO2}$ ratio: Implications for total stratospheric Br_y and bromine-mediated ozone loss. *Atmos. Chem. Phys.*, *13*(13), 6263–6274. doi: 10.5194/acp-13-6263-2013

Krotkov, N. A., Lamsal, L. N., Celarier, E. A., Swartz, W. H., et al. (2017). The version 3 OMI NO_2 standard product. *Atmos. Meas. Tech. Discuss.*, (2), 1–42. doi: 10.5194/amt-2017-44

Levelt, P. F., Van den Oord, G. H. J., Dobber, M. R., Malkki, A., et al. (2006). The Ozone Monitoring Instrument. *IEEE Trans. Geosci. Remote Sens.*, *44*(5), 1093–1101. doi: Urn:nbn:nl:ui:25-648485

Liang, Q., Atlas, E., Blake, D., Dorf, M., et al. (2014). Convective transport of very short lived bromocarbons to the stratosphere. *Atmos. Chem. Phys.*, *14*(11), 5781–5792. doi: 10.5194/acp-14-5781-2014

Malicet, J., Daumont, D., Charbonnier, J., Parisse, C., et al. (1995). Ozone UV spectroscopy. II. Absorption cross-sections and temperature dependence. *J. Atmos. Chem.*, *21*(3), 263–273. doi: 10.1007/BF00696758

McElroy, M. B., Salawitch, R. J., Wofsy, S. C., & Logan, J. A. (1986). Reductions of Antarctic ozone due to synergistic interactions of chlorine and bromine. *Nature*, *321*(6072), 759–762. doi: 10.1038/321759a0

McLinden, C. A., Haley, C. S., Lloyd, N. D., Hendrick, F., et al. (2010). Odin/OSIRIS observations of stratospheric BrO: Retrieval methodology, climatology, and inferred Br_y. *J. Geophys. Res. Atmos.*, *115*(15), 1–19. doi: 10.1029/2009JD012488

Meller, R., & Moortgat, G. K. (2000). Temperature dependence of the absorption cross sections of formaldehyde between 223 and 323 K in the wavelength range 225-375 nm. *J. Geophys. Res. Atmos.*, *105*(D6), 7089–7101. doi: 10.1029/1999JD901074

Millán, L., Livesey, N., Read, W., Froidevaux, L., et al. (2012). New Aura Microwave Limb Sounder observations of BrO and implications for Bry. *Atmos. Meas. Tech.*, *5*(7), 1741–1751. doi: 10.5194/amt-5-1741-2012

Montzka, S. A., Reimann, S., Engel, A., Krüger, K., et al. (2011). Ozone-depleting substances (ODSs) and related chemicals, Chapter 1. In *Scientific Assessment of Ozone Depletion: 2010, Global Ozone Research and Monitoring Project – Report No. 52* (52nd ed.). Geneva, Switzerland: World Meteorological Organization.

Neuman, J. A., Nowak, J. B., Huey, L. G., Burkholder, J. B., et al. (2010). Bromine measurements in ozone depleted air over the Arctic Ocean. *Atmos. Chem. Phys.*, *10*(14), 6503–6514. doi: 10.5194/acp-10-6503-2010

Parrella, J. P., Chance, K., Salawitch, R. J., Canty, T., et al. (2013). New retrieval of BrO from SCIAMACHY limb: An estimate of the stratospheric bromine loading during April 2008. *Atmos. Meas. Tech.*, *6*(10), 2549–2561. doi: 10.5194/amt-6-2549-2013

Peterson, P. K., Simpson, W. R., Pratt, K. A., Shepson, P. B., et al. (2015). Dependence of the vertical distribution of bromine monoxide in the lower troposphere on meteorological factors such as wind speed and stability. *Atmos. Chem. Phys.*, *15*(4), 2119–2137. doi: 10.5194/acp-15-2119-2015

Platt, U., & Stutz, J. (2008). *Differential Optical Absorption Spectroscopy*.

Prados-Roman, C., Butz, A., Deutschmann, T., Dorf, M., et al. (2011). Airborne DOAS limb measurements of tropospheric trace gas profiles: Case studies on the profile retrieval of O4 and BrO. *Atmos. Meas. Tech.*, *4*(6), 1241–1260. doi: 10.5194/amt-4-1241-2011

Rienecker, M. M., Suarez, M. J., Gelaro, R., Todling, R., et al. (2011). MERRA: NASA's

Modern-Era Retrospective Analysis for Research and Applications. *J. Clim.*, *24*(14), 3624–3648. doi: 10.1175/JCLI-D-11-00015.1

Rozanov, A., Rozanov, V., Buchwitz, M., Kokhanovsky, A., & Burrows, J. P. (2005). SCIATRAN 2.0 – A new radiative transfer model for geophysical applications in the 175–2400nm spectral region. *Adv. Sp. Res.*, *36*(5), 1015–1019. doi: 10.1016/j.asr.2005.03.012

Saiz-Lopez, A., & von Glasow, R. (2012). Reactive halogen chemistry in the troposphere. *Chem. Soc. Rev.*, *41*(19), 6448. doi: 10.1039/c2cs35208g

Salawitch, R. J., Canty, T., Kurosu, T., Chance, K., et al. (2010). A new interpretation of total column BrO during Arctic spring. *Geophys. Res. Lett.*, *37*(21), 1–9. doi: 10.1029/2010GL043798

Salawitch, R. J., Weisenstein, D. K., Kovalenko, L. J., Sioris, C. E., et al. (2005). Sensitivity of ozone to bromine in the lower stratosphere. *Geophys. Res. Lett.*, *32*(5), L05811. doi: 10.1029/2004GL021504

Sander, S. P., Friedl, R. R., Golden, D. M., Kurylo, M. J., et al. (2011). *Chemical Kinetics and Photochemical Data for Use in Atmospheric Studies, Evaluation No. 17," JPL Publication 10-6, Jet Propulsion Laboratory, Pasadena*. *JPL Publication 10-6*. https://doi.org/10.1002/kin.550171010

Sander, S. P., Ray, G. W., & Watson, R. T. (1981). Kinetics Study of the Pressure Dependence of the BrO + NO_2 Reaction at 298 K. *J. Phys. Chem*, *85*(2), 199–210.

Schmidt, J. A., Jacob, D. J., Horowitz, H. M., Hu, L., et al. (2016). Modeling the observed tropospheric BrO background: Importance of multiphase chemistry and implications for ozone, OH, and mercury. *J. Geophys. Res. Atmos.*, *121*(19), 11,819-11,835. doi: 10.1002/2015JD024229

Schofield, R., Johnston, P. V., Thomas, A., Kreher, K., et al. (2006). Tropospheric and stratospheric BrO columns over Arrival Heights, Antarctica, 2002. *J. Geophys. Res.*, *111*(D22), D22310. doi: 10.1029/2005JD007022

Schofield, R., Kreher, K., Conner, B. J., Johnston, P. V., et al. (2004). Retrieved tropospheric and stratospheric BrO columns over Lauder, New Zealand. *J. Geophys. Res.*, *109*(D14), D14304. doi: 10.1029/2003JD004463

Seo, S., Richter, A., Blechschmidt, A., Bougoudis, I., & Burrows, J. P. (2018). First high resolution BrO column retrievals from TROPOMI. *Atmos. Meas. Tech. Discuss.*, (December), 1–26. doi: 10.5194/amt-2018-365

Simpson, W. R., Brown, S. S., Saiz-Lopez, A., Thornton, J. A., & Von Glasow, R. (2015). Tropospheric Halogen Chemistry: Sources, Cycling, and Impacts. *Chem. Rev.*, *115*(10), 4035–4062. doi: 10.1021/cr5006638

Simpson, W. R., Peterson, P. K., Frieß, U., Sihler, H., et al. (2017). Horizontal and vertical structure of reactive bromine events probed by bromine monoxide MAX-DOAS. *Atmos. Chem. Phys.*, *17*(15), 9291–9309. doi: 10.5194/acp-17-9291-2017

Sinnhuber, B.-M., Rozanov, A., Sheode, N., Afe, O. T., et al. (2005). Global observations of stratospheric bromine monoxide from SCIAMACHY. *Geophys. Res. Lett.*, *32*(20), L20810. doi: 10.1029/2005GL023839

Sinnhuber, B. M., & Meul, S. (2015). Simulating the impact of emissions of brominated very short lived substances on past stratospheric ozone trends. *Geophys. Res. Lett.*, *42*(7), 2449–2456. doi: 10.1002/2014GL062975

Sioris, C. E., Kovalenko, L. J., McLinden, C. A., Salawitch, R. J., et al. (2006). Latitudinal and vertical distribution of bromine monoxide in the lower stratosphere from Scanning Imaging

Absorption Spectrometer for Atmospheric Chartography limb scattering measurements. *J. Geophys. Res.*, *111*(D14), D14301. doi: 10.1029/2005JD006479

SPARC. (2010). *SPARC CCMVal Report on the Evaluation of Chemistry-Climate Models* (WCRP-132,). (D. W. W. V. Eyring, T. G. Shepherd, Ed.), *SPARC Report No. 5, WCRP-30/2010,WMO/TD-No.40*. Retrieved from http://www.atmosp.physics.utoronto.ca/SPARC/News15/15_Udelhofen.html

Spinei, E., Carn, S. A., Krotkov, N. A., Mount, G. H., et al. (2010). Validation of ozone monitoring instrument SO_2 measurements in the Okmok volcanic cloud over Pullman, WA, July 2008. *J. Geophys. Res. Atmos.*, *115*(18), 1–14. doi: 10.1029/2009JD013492

Spinei, E., Cede, A., Swartz, W. H., Herman, J., & Mount, G. H. (2014). The use of NO_2 absorption cross section temperature sensitivity to derive NO<sub>2>/sub> profile temperature and stratospheric-tropospheric column partitioning from visible direct-sun DOAS measurements. *Atmos. Meas. Tech.*, *7*(12), 4299–4316. doi: 10.5194/amt-7-4299-2014

Spurr, R. J. D., Kurosu, T. P., & Chance, K. V. (2001). A linearized discrete ordinate radiative transfer model for atmospheric remote-sensing retrieval. *J. Quant. Spectrosc. Radiat. Transf.*, *68*(6), 689–735. doi: 10.1016/S0022-4073(00)00055-8

Stachnik, R. A., Millán, L., Jarnot, R., Monroe, R., et al. (2013). Stratospheric BrO abundance measured by a balloon-borne submillimeterwave radiometer. *Atmos. Chem. Phys.*, *13*(6), 3307–3319. doi: 10.5194/acp-13-3307-2013

Strahan, S. E., Duncan, B. N., & Hoor, P. (2007). Observationally derived transport diagnostics for the lowermost stratosphere and their application to the GMI chemistry and transport model. *Atmos. Chem. Phys.*, *7*, 2435–2445. doi: 10.5194/acpd-7-1449-2007

Stutz, J., & Platt, U. (1996). Numerical analysis and estimation of the statistical error of differential optical absorption spectroscopy measurements with least-squares methods. *Appl. Opt.*, *35*(30), 6041–6053.

Stutz, J., Werner, B., Spolaor, M., Scalone, L., et al. (2017). A new Differential Optical Absorption Spectroscopy instrument to study atmospheric chemistry from a high-altitude unmanned aircraft. *Atmos. Meas. Tech.*, *10*(3), 1017–1042. doi: 10.5194/amt-10-1017-2017

Suleiman, R. M., Chance, K., Liu, X., González Abad, G., et al. (2019). OMI total bromine monoxide (OMBRO) data product: algorithm, retrieval and measurement comparisons. *Atmos. Meas. Tech.*, *12*(4), 2067–2084. doi: 10.5194/amt-12-2067-2019

Theys, N., Van Roozendael, M., Errera, Q., Hendrick, F., et al. (2009). A global stratospheric bromine monoxide climatology based on the BASCOE chemical transport model. *Atmos. Chem. Phys.*, *9*(3), 831–848. doi: 10.5194/acp-9-831-2009

Theys, N., Van Roozendael, M., Hendrick, F., Fayt, C., et al. (2007). Retrieval of stratospheric and tropospheric BrO columns from multi-axis DOAS measurements at Reunion Island (21° S, 56° E). *Atmos. Chem. Phys.*, *7*(18), 4733–4749. doi: 10.5194/acp-7-4733-2007

Theys, N., Van Roozendael, M., Hendrick, F., Yang, X., et al. (2011). Global observations of tropospheric BrO columns using GOME-2 satellite data. *Atmos. Chem. Phys.*, *11*(4), 1791–1811. doi: 10.5194/acp-11-1791-2011

Thorn, R. P., Daykin, E. P., & Wine, P. H. (1993). Kinetics of the BrO + NO_2 Association Reaction. Temperature and Pressure Dependence in the Falloff Regime. *Int. J. Chem. Kinet.*, *25*, 521–537.

Tilmes, S., Kinnison, D. E., Garcia, R. R., Salawitch, R., et al. (2012). Impact of very short-lived halogens on stratospheric ozone abundance and UV radiation in a geo-engineered atmosphere. *Atmos. Chem. Phys.*, *12*, 10945–10955. doi: 10.5194/acp-12-10945-2012

Tzortziou, M., Herman, J. R., Cede, A., & Abuhassan, N. (2012). High precision, absolute total column ozone measurements from the Pandora spectrometer system: Comparisons with data from a Brewer double monochromator and Aura OMI. *J. Geophys. Res. Atmos.*, *117*(16), 1–14. doi: 10.1029/2012JD017814

Van Roozendael, M., Wagner, T., Richter, A., Pundt, I., et al. (2002). Intercomparison of BrO measurements from ERS-2 GOME, ground-based and balloon platforms. *Adv. Sp. Res.*, *29*(11), 1661–1666. doi: 10.1016/S0273-1177(02)00098-4

Vandaele, A. C., Hermans, C., Simon, P. C., Carleer, M., et al. (1998). Measurements of the NO_2 absorption cross-section from 42 000 cm^{-1} to 10 000 cm^{-1} at 220 K and 294 K. *J. Quan. Spectrosc. Radiat. Transf.*, *59*, 171–184.

Veefkind, J. P., Bhartia, P. K., Gleason, J., de Haan, J. F., et al. (2006). Total Ozone from the Ozone Monitoring Instrument (OMI) using TOMS and DOAS Methods. *IEEE Trans. Geosci. Remote Sens.*, *44*(5), 8932.

Vogel, L., Sihler, H., Lampel, J., Wagner, T., & Platt, U. (2013). Retrieval interval mapping: a tool to visualize the impact of the spectral retrieval range on differential optical absorption spectroscopy evaluations. *Atmos. Meas. Tech.*, *6*(2), 275–299. doi: 10.5194/amt-6-275-2013

Wagner, T., Leue, C., Wenig, M., Pfeilsticker, K., & Platt, U. (2001). Spatial and temporal distribution of enhanced boundary layer BrO concentrations measured by the GOME instrumnet aboard ERS-2. *J. Geophys. Res.*, *106*, 24225–24235. doi: https://doi.org/10.1029/2000JD000201

Wagner, T., & Platt, U. (1998). Satellite mapping of enhanced BrO concentrations in the troposphere. *Nature*, *395*(6701), 486–490. doi: 10.1038/26723

Wahner, A., Tyndall, G. S., & Ravishankara, A. R. (1987). Absorption cross sections for symmetric chlorine dioxide as a function of temperature in the wavelength range 240-480nm. *J. Phys. Chem.*, *91*(11), 2734–2738. doi: 10.1021/j100295a018

Wales, P. A., Salawitch, R. J., Nicely, J. M., Anderson, D. C., et al. (2018). Stratospheric Injection of Brominated Very Short-Lived Substances: Aircraft Observations in the Western Pacific and Representation in Global Models. *J. Geophys. Res. Atmos.*, *123*(10), 5690–5719. doi: 10.1029/2017JD027978

Wamsley, P. R., Elkins, J. W., Fahey, D. W., Dutton, G. S., et al. (1998). Distribution of halon-1211 in the upper troposphere and lower stratosphere and the 1994 total bromine budget. *J. Geophys. Res. Atmos.*, *103*(D1), 1513–1526. doi: 10.1029/97JD02466

Wetzel, G., Oelhaf, H., Höpfner, M., Friedl-Vallon, F., et al. (2017). Diurnal variations of $BrONO_2$ observed by MIPAS-B at midlatitudes and in the Arctic. *Atmos. Chem. Phys.*, *17*(23), 14631–14643. doi: 10.5194/acp-17-14631-2017

Wilmouth, D. M., Hanisco, T. F., Donahue, N. M., & Anderson, J. G. (1999). Fourier Transform Ultraviolet Spectroscopy of the A 2Π3/2 ← X 2Π3/2 Transition of BrO. *J. Phys. Chem. A*, *103*(45), 8935–8945. doi: 10.1021/jp991651o

Wofsy, S. C., McElroy, M. B., & Yung, Y. L. (1975). The chemistry of atmospheric bromine. *Geophys. Res. Lett.*, *2*(6), 215–218. doi: 10.1029/GL002i006p00215

World Meteorological Organization. (1957). Meteorology—A three-dimensional science: Second session of the Commission for Aerology. *WMO Bull.*